LAPPEENRANTA UNIVERSITY OF TECHNOLOGY
Faculty of Technology
Degree Programme in Electrical Engineering

Master's Thesis

Manu Niukkanen

Design of an amplifier and an instrumentation setup for a harsh environment heat flux measurement application – case axial flux electric machine

Examiners: Professor Pertti Silventoinen
D.Sc.(tech) Mikko Kuisma

ABSTRACT

Lappeenranta University of Technology
Faculty of Technology
Degree Programme in Electrical Engineering

Manu Niukkanen

Design of an amplifier and an instrumentation setup for a harsh environment heat flux measurement application – case axial flux electric machine

2013

Master's Thesis.
82 p., 39 figures, 3 tables, 4 appendixes.

Examiner: Professor Pertti Silventoinen
D.Sc.(tech) Mikko Kuisma

Keywords: heat flux sensor, instrumentation, transverse Seebeck effect, amplifier

Measurement is a tool for researching. Therefore, it is important that the measuring process is carried out correctly, without distorting the signal or the measured event. Researches of thermoelectric phenomena have been focused more on transverse thermoelectric phenomena during recent decades. Transverse Seebeck effect enables to produce thinner and faster heat flux sensor than before. Studies about transverse Seebeck effect have so far focused on materials, so in this Master's Thesis instrumentation of transverse Seebeck effect based heat flux sensor is studied,

This Master's Thesis examines an equivalent circuit of transverse Seebeck effect heat flux sensors, their connectivity to electronics and choosing and design a right type amplifier. The research is carried out with a case study which is Gradient Heat Flux Sensors and an electrical motor.

In this work, a general equivalent circuit was presented for the transverse Seebeck effect-based heat flux sensor. An amplifier was designed for the sensor of the case study, and the solution was produced for the measurement of the local heat flux of the electric motor to improve the electromagnetic compatibility.

TIIVISTELMÄ

Lappeenrannan teknillinen yliopisto
Teknillinen tiedekunta
Sähkötekniikan koulutusohjelma

Manu Niukkanen

Vahvistimen ja instrumentoinnin suunnittelu häiriöiseen ympäristöön lämpövuon mittauksiin – case aksiaalivuosähkömoottori

2013
Diplomityö.
82 s., 39 kuvaa, 3 taulukkoa, 4 liitettä.

Tarkastaja: Professori Pertti Silventoinen
TkT Mikko Kuisma
Hakusanat: lämpövuoanturi, instrumentointi, vahvistin, poikittainen Seebeck ilmiö

Mittaaminen on yksi tutkimustyökaluista. Siksi onkin tärkeää, että mittaustapahtuma suoritetaan oikein ja mittalaite toimii oikealla periaatteella mittaustapahtumaa ja anturin signaalia vääristämättä. Lämpösähköisten ilmiöiden tutkimus on viime vuosikymmeninä keskittynyt yhä enemmän poikittaisiin lämpösähköisiin ilmiöihin. Poikittainen Seebeck-ilmiö mahdollistaa entistä nopeiden ja ohuempien lämpövuoantureiden valmistamisen. Tutkimukset ovat tähän asti keskittyneet materiaalitutkimuksiin ja sen vuoksi tässä diplomityössä tutkitaan poikittais Seebeck-ilmiöön perustuvien lämpövuoanturien instrumentointia.

Tässä diplomityössä tutkitaan gradientti lämpövuoanturien avulla esimerkkitapauksen kautta poikittaisen Seebeck-ilmiöön perustuvien lämpövuoanturien sijaiskytkentää, liittämistä elektroniikkaan, oikean tyyppisen vahvistimen valintaan ja suunnitteluun, sekä tutkitaan mittausympäristön vaikutusta instrumentointiin. Tutkimuskohteena on aksiaalivuosähkömoottori, jota on tutkittu aikaisemmin mittaamalla ilmavälin lämpövuota.

Tuloksina tässä työssä esitetään yleinen sijaiskytkentä poikittaiseen Seebeck-ilmiöön perustuville lämpövuoantureille. Antureille suunniteltiin vahvistin sähkömoottorin ilmavälin lämpövuon mittausta varten, sekä tuotettiin ratkaisumalli sähkömoottorissa mittaamisen sähkömagneettisen yhteensopivuuden parantamiseksi.

PREFACE

This Master's Thesis was made for Lappeenranta University of Technology department of LUT Energia as the final work of my studies.

I want to thank Professor Pertti Silventoinen for offering this work for me and examining this work. I want to thank D.Sc.(tech) Mikko Kuisma for guidance during this work and being the second examiner. I want to thank the Head of LUT Energy, Professor Jarmo Partanen for funding this thesis work. Many thanks for D.Sc.(tech) Hanne Jussila for helping with the measurements and Professor Andrey Mityakov for providing the sensor and information of the sensor. I also want to thank M.Sc.(tech) Joonas Talvitie and M.Sc.(tech) Juho Montonen for reviewing and commenting this work.

I would like to extend my warmest thanks to my parents Jyrki and Marja and my brother Simo for endless support during my student years.

Lappeenranta, March 25th, 2013

Manu Niukkanen

CONTENTS

NOMENCLATURE

A	Material A
ADC	Analog to Digital Converter
AT	Anisotropic Thermoelement
B	Material B
BSCCO	Bishmuth Strontium Calium Copper oxide, $Bi_2Sr_2CaCu_2O_8$ –film
BW	Bandwidth
CMRR	Common Mode Rejection Ratio
DAQ	Data Acquisition device
EMC	Electro magnetic compatibility
EMI	Electro magnetic interference
emf	electromagnetic force
GHFS	Gradient heat flux sensor
HFS	Heat Flux Sensor
IC	Integrated Circuit
LPF	Low pass filter
PCB	Printed Circuit Board
PM	Permanent Magnet
PSRR	Power Supply Rejection Ratio
RFI	Radio Frequency Interference
RLC	Resistance-Inductance-Capacitance circuit
V+	Non-inverting input pin
V-	Inverting input pin
YBCO	Yttrium Barium Copper Oxide, $YBa_2Cu_3O_{7-\delta}$ film

A	area
$\boldsymbol{B}$	magnetic field
C	capacitance
$\boldsymbol{E}$	electric field
f	frequency
G	gain
I	electric current
j	current density
k	Boltzman’s coefficient
L	inductance
l	length

q	thermal power, Peltier heat
q''	heat flux
R	resistance, reluctance, R_m
S	Seebeck coefficient
s	Laplace variable
t	tolerance
T	temperature
U	voltage
V	voltage
Z	impedance

α	angle
δ	skin depth
λ	wavelength
μ	permeability
Π	Peltier coefficient
τ	time constant
θ	angle

Subscripts

A	Area
AB	materials A and B
B	magnetic flux
amp	amplifier
C	Capacitance
ca	cable
cl	closed loop
rms	root-mean-square, tehollisarvon kuvaus
f	feedback
i	i.th term
in	input
io	input offset
load	load
n	noise, n:th term
ol	open loop
out	output

s	sensor
S	Seebeck
P	Peltier
rms	Root Mean Squared
tP	transverse Peltier effect
tS	transverse Seebeck effect
th	thermal

1 INTRODUCTION

Lord Kelvin said once that "--when you can measure what you are speaking about, and express it in numbers, you know something about it--". Measuring is a way to gather knowledge and a tool for proofing. Measuring should be made reliably to fulfill its purpose. Physical signal which is wanted to be measured needs to be converted to electrical signal. Sensors are devices that convert physical signal into electrical signal and using that sensor to measurement is called instrumentation. When a reliable measurement is performed, one needs to be sure that the instrumentation should not alter the event being measurement [1]. As well the instrumentation should not alter the sensor signals. Usually sensors are not capable to produce electrical signal that can be displayed directly as the value it has measured. Signal conditioning is needed to fit the sensor and its reading unit together, which all together are an instrument.

It is important that the measuring input of signal conditioner is receiving only the signal of the sensor. Therefore, instrumentation takes a stand also to signal fidelity, an instrumentation environment and electromagnetic compatibility (EMC). It is important that signal is not altered in signal conditioning. The instrumentation should survive the environmental load and produce output as accurate as possible.

A signal chain for an instrument should be defined to see what building blocks the instrumentation needs. In figure 1.1 is a typical signal chain of an instrument. Building blocks of a signal chain receives signal from another block and transmit to the next block. [2]

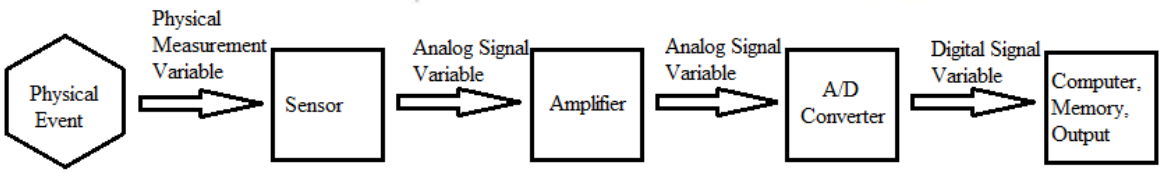

Figure 1.1 An example of signal chain in an instrument. Modified from [2].

The amplifier in figure 1.1 is a simple version of a signal condition unit which is an important block of a signal chain. Signal conditioners, which contain filters, amplifiers and other analog processing unit to produce compatible signal for the reading unit, which are nowadays mostly analog to digital converters (ADC) connected to a microprocessor. Analog signal conditioners can also perform mathematical operations or conversions like linear or logarithmic actions [1].

It is important for a designer to know what for the instrument is made. Especially when choosing the sensor to measure the physical signal. Instrumentation of heat flux based on a new type of sensor is studied in this thesis. In some industrial applications, heat flux is more important to know than temperature. Especially in heat transfer application. According to second law of thermodynamics, thermal energy transfers from warmer to colder temperature. Heat transfer occurs when a temperature gradient/difference exists. Heat flux is a thermodynamic quantity which describes amount of heat current applied through a plane. In practice it is thermal power transferred per surface area. The unit for heat flux is watts per square meter, W/m^2. Heat flux is affected to the direction where temperature difference ΔT exists. [3] [4]

The one way to measure heat flux, without specific heat flux sensor (HFS) is to measure temperature both side of medium under inspection with known thickness and thermal conductivity then calculate the heat flux by Fourier's law (1.1) [3] [4] [5]

$$q'' = -\frac{R_{\mathrm{th}}\Delta T}{l} \tag{1.1}$$

where R_{th} is thermal resistivity and ΔT is temperature difference of surfaces and l the length between surfaces. If the thermal capacitance of the material is known, temperature measurement over time will also produce the value of heat flux. This isn't very practical method and it is indirect way to measure heat flux. Also it can be relatively slow if materials have large heat capacity which means that temperature changes are slower when heat capacitance is larger. [3] Characteristic to heat flux is temperature differences. This sets limitations to instrumentation. For a heat flux measurement, electronics is needed to be able to tolerate temperature changes of an ambient and also to operate possible relatively high temperatures, if sensor and signal conditioning unit can't be separated.

Heat flux sensors studied in this Thesis are based on transverse Seebeck effect. [6] This less known thermoelectric effect appears in thermoelectrically anisotropic materials. Thermocouple is based on the traditional longitudinal Seebeck effect where electric fields and temperature differences are collinear. Transverse Seebeck effect is thermoelectric effect which is proportional to a temperature gradient perpendicular to the generated electric field. In the literature, there is no study about the instrumentation of transverse Seebeck effect at the moment of writing this thesis, but only researches about the phenomenon itself and thermoelectric materials. On the other hand, the most of the material studies have documentation about the measuring event.

1.1 The Case

In this thesis an instrumentation of a heat flux sensor based on transverse Seebeck effect is studied in measurement of local heat flux of the air gap of an axial flux electric motor. In Lappeenranta University of Technology local heat flux of an electric motor has been studied [6]. The heat transfer in an electrical machine is studied because it affects to the performance of the motor. Thermal analysis of an axial flux permanent magnet machine is related to the maximum power output of the machine. [7] Currently thermal modeling of the rotor is made with computer analysis and indirect measurements with temperature sensors. [6] Neodymium iron boron permanent magnets (PM) represent the latest development of the permanent magnets. They are used in modern electrical motors. Unfortunately neodymium iron boron magnets demagnetizes at relatively low temperature at circa 100…150 ^{0}C. [7][8][9] The thermal design is then as important as the electrical design in PM-motors [8][9].

There are not much suitable sensors available for measuring local heat flux in electrical motors. [6] Recent development in study of transverse Seebeck effect enables to produce heat flux sensors which could fit to an air gap of an electric motor. Two of these new types of the heat flux sensors are attached on a stator iron and a stator slot wedge in the air gap of axial flux permanent magnet motor. Previous test showed that a measuring instrument couldn't always or not at all measure the output voltages of the sensors when the motor was running. Reported issues were possible ground loops and common mode voltage because the sensor became readable when motor was turned off and rotor was still rotating. Also sensors' low output voltage was problem for a capable measuring device.

The electric motor is an axial flux permanent magnet motor with two stator stacks and ironless rotor with 10 rotor poles and 12 stator slots per side. Permanent magnets are made from neodymium iron boron. In the Appendix I, can be seen the main parameters of the motor.

The environment in the electrical motor for the electronics is quite harsh. The sensors are placed on a stator tooth and a stator slot in the air gap of the motor which is 2.0 mm wide. Temperature at maximum load could reach over 90 ^{0}C and high magnetic flux even 1 T and higher is present. In the measurement performed by Jussila et al [6], the machine reached temperature of 65 ^{0}C at no load.

There is little knowledge, what kind of dynamic signal the heat flux in the air gap of the motor produces. Jussila et al measured only DC values at their tests. DC might not be enough, so the signal bandwidth for local heat flux measurement in the electrical motor is

set to be from direct current (DC) to ten times the frequency of magnets at the nominal speed, which yields 4 kHz.

1.2 Goals of Thesis

The goals for this thesis are to study instrumentation of transverse Seebeck effect heat flux sensors and their implementation to harsh environment application based on the case. The instrumentation issues are to find electrical model for a transverse Seebeck heat flux sensor and proper signal conditioning and amplifier. The goals for the case study are solving electromagnetic issues and specifying a signal chain for instrumentation and design an amplifier for signal conditioning.

Research methods used in this Master's Thesis are model based problem solving. Models were acquired from literature and measurements. Problems were solved with the models by using measurements and simulations.

1.3 Structure

This thesis continues after this introduction as follow. Chapter 2 introduces basics of thermoelectricity and theory of transverse thermoelectric effects. Chapter 2 also contains the electrical theory needed in this thesis, which includes electromagnetism, electromagnetic compatibility, circuit theory and introduction about amplifiers and their circuits. In chapter 3, studies about transverse Seebeck effect sensors is reviewed and studied for making an electrical model for them. Chapter 4 is the case oriented part of this thesis, where the instrumentation problems of the case are studied, which solutions are presented, and an amplifier design is made for GHFS in the case. The fifth chapter is the conclusion of this thesis.

2 THEORY

In addition to knowing what to measure it also needed to know how sensors can produce the measurement and how it is used properly. Also it is good to know what kind of other phenomena can alter sensors and signal, and of course can these affect to the signal conditioning unit. In this chapter thermoelectric phenomena are introduced. Theory of EMC and amplifiers needed in this thesis, are after thermoelectric phenomena.

2.1 Thermoelectric effects

Thermoelectric effects are phenomena which describes the relationship between the heat flow and electricity due to material properties. Heat generated by power loss in resistance doesn't include thermoelectric effect. This *Joule heating* is not reversible, like thermoelectric effects, and it is not proportional to any temperature or temperature gradient. [10] The basic thermoelectric effects are Seebeck, Peltier and Thomson effects. There are also transverse phenomena for Seebeck and Peltier effects.

2.1.1 Seebeck effect

The science of thermoelectricity began when Thomas Seebeck discovered a phenomenon, where voltage is generated by two dissimilar conductors having temperature difference at their junction. Seebeck published his research in 1823. [11] [12] The phenomenon was named after its founder as the Seebeck effect. Figure 2.1 shows the voltage generation by Seebeck effect. The structure of the connection is called thermocouple. The circuit has two dissimilar conductors (or semiconductors) A and B. If temperatures T_1 and T_2 are same, then there is no voltage difference. When temperatures aren't the same, then it thermoelectromotive force (emf) is created.

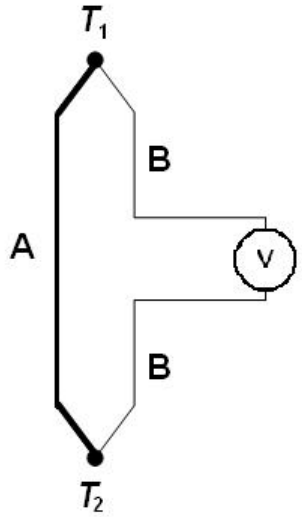

Figure 2.1 Basic thermocouple circuit. Conductors A and B are different material. When there are temperature difference at points T_1 and T_2, it can be read with the voltage meter. Modified from [10]

The thermocouple conductors need to be different material to create the seebeck effect, if the conductors A and B are same material, thermo-emf generated cancel each other out. Voltage generated by per unit temperature difference in material is called the Seebeck coefficient S [$\mu V/^0C$]. [13] Every material has its own Seebeck coefficient which is proportional to the Seebeck coefficient of platinum. Equation for Seebeck voltage is:

$$U = S_{AB} * \Delta T, \tag{2.1}$$

where S_{AB} is combined Seebeck coefficient of thermocouple materials A and B respectively. [13] [14]Thermocouples are used in temperature measurements. The cold junction temperature has to be known and compensated for the measurement of the actual temperature. Thermocouples have the widest temperature range than other thermal sensor technologies, -200 to +2315 degrees. [15] Seebeck effect is also used in thermopiles where are multiple thermocouple connected together. Thermopiles are used in heat flux sensors.

2.1.2 Peltier effect

Peltier effect was discovered by Jean Peltier in 1834. In the other hand Lenz explained the true nature of the Peltier effect in 1838. [13][14] Peltier effect is opposite phenomenon to Seebeck effect. Like in the Seebeck effect Peltier effect occurs when two dissimilar conductors or semiconductors are present. Peltier effect creates the temperature difference to the junctions when electric current is applied through the dissimilar conductors. Heat can be absorbed or liberated with Peltier effect [14] Figure 2.2 shows the Peltier circuit.

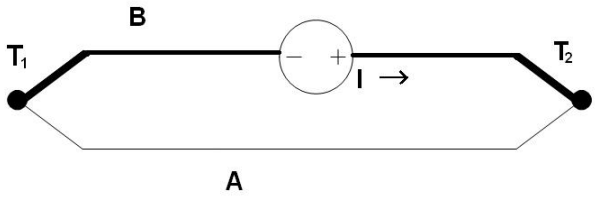

Figure 2.2 Peltier-element circuit. Conductors A and B are different materials. When current is applied to the circuit temperature will differences at points T_1 and T_2.

The temperature difference between junctions in figure 2.2 is related to direction of the current. The same junction can be a cooler or a heater depending on the direction of the electric current. Material's ability to Peltier effect is descripted with the Peltier coefficient π_P. Equation for Peltier effect is

$$q = I\pi_P \tag{2.2}$$

where q is Peltier heat and I is applied current. Peltier effect is mostly used in solid state coolers. [13] Because their low efficiency they are rare compared to traditional cooling devices. Advantages of Peltier coolers are light weight and low need of service. [12]

2.1.3 Thomson effect

Lord Kelvin (also known as William Thomson) discovered Thomson effect and was named after him in 1851. Thomson effect describes heating or cooling in current carrying conductor with different temperatures at two points. [13] Materials have their own coefficient to Thomson effects.

Since the Seebeck effect creates electromotive force (emf) which drives the electric current to the circuit. The current enables Peltier and Thomson effects to occur and may introduce temperature errors. Though that error is not significant and it is smaller compared to voltage losses in resistance [14] [16]

2.2 Transverse thermoelectric effects

Lord Kelvin was also the first to discover transverse thermoelectric effects on materials [17] [12]. Nevertheless, studies of thermoelectric have been concentrated to longitudinal

thermoelectric effects. [12][5] In Seebeck and Peltier effects the thermo electricity is proportional with longitudinal temperature difference but transverse thermoelectric fields and temperature gradients are perpendicular to each other. [12][18] The transverse effects are observable when a material has anisotropic Seebeck coefficient [16] [18]. From figure 2.3 can be seen the relation of electric and heat vectors in both longitudinal and transverse thermoelectric effects.

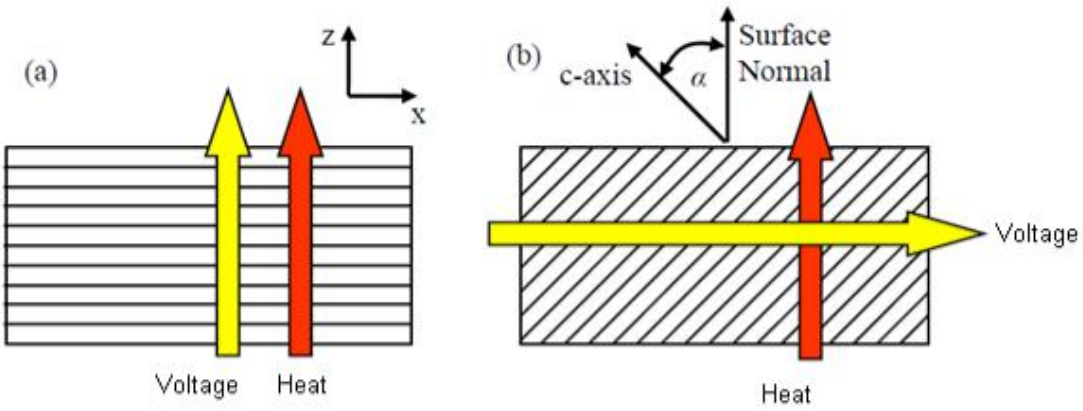

Figure 2.3 Difference between heat and thermo-emf in a) thermoelectric effect b) transverse thermoelectric effect. Modified from [12].

When the material is tilted and cut, with an angle α along the c -axis, the material changes to thermoelectrically anisotropic. Figure 2.3 is same for the Peltier effect when voltage is replaced with current density. An anisotropic property is whether intrinsic structure of a material or artificially formed by layering two different material.[10][16][18] In figure 2.4 is presented both intrinsic and anisotropic material structure.

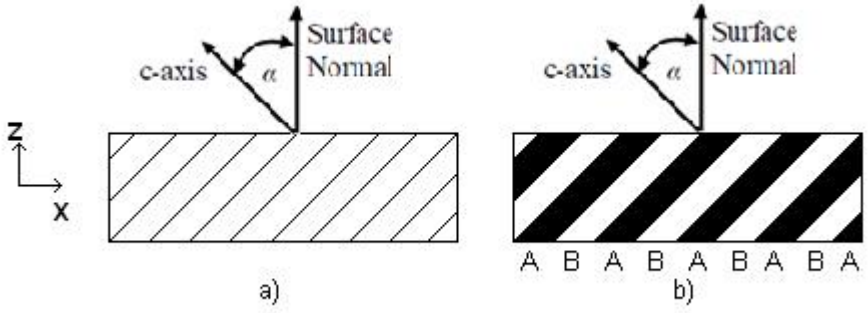

Figure 2.4 Transverse thermoelectric element constructions, a) intrinsic anisotropic material b) artificial anisotropic multilayer structure made from materials A and B.

As can be seen from figure 2.4 that intrinsic and artificial thermoelectric materials have the same structure but artificial is created from two different materials like a thermocouple to mimic an intrinsic thermoelectric material.

Transverse Seebeck effect creates thermo-emf proportional to temperature gradient ∇T and Seebeck coefficient $\boldsymbol{S}$ which is proportional to materials in used and the angle α. Equation for electric field generated by transverse Seebeck effect in the equation (2.3) [10][16][18]

$$\boldsymbol{E}_{\mathrm{th}} = \boldsymbol{S}\nabla T \tag{2.3}$$

Where $\boldsymbol{S}$ is Seebeck tensor matrix which is tells longitudinal and transverse components of the Seebeck coefficient of direction of x, y and z. The Seebeck tensor matrix is presented in (2.4). [10][16][18][19]

$$\boldsymbol{S} = \begin{bmatrix} S_{\parallel}\cos^2\alpha + S_{\perp}\sin^2\alpha & 0 & \frac{1}{2}(S_{\parallel} - S_{\perp})\sin 2\alpha \\ 0 & S_{\parallel} & 0 \\ \frac{1}{2}(S_{\parallel} - S_{\perp})\sin 2\alpha & 0 & S_{\parallel}\cos^2\alpha + S_{\perp}\sin^2\alpha \end{bmatrix} \tag{2.4}$$

Where α is the angle of crystallographic axel, $S_{\parallel}$ is longitudinal Seebeck coefficient and $S_{\perp}$ is transverse Seebeck coefficient. While the output of transverse Seebeck effect is generated by heat flux, respect to length of anisotropic material in x - axel direction, where the heat flux in z - axel direction is applied.

$$U_{\mathrm{th}} = E_{\mathrm{th}} l_{\mathrm{x}} \tag{2.5}$$

This is also the princible of longitudinal Seebeck effect in thermocouples, but the length considered in the equation (2.5) is decremented by substitution of ∇T with equivalent ΔT and length l. Although the anisotropic materials, intrinsic or artificial are made to maximize the transversal component of the Seebeck effect to generate thermo-emf of transverse Seebeck effect, longitudinal Seebeck effect is still observable when measuring leads are different material than the sensor. This can be seen from the matrix (2.4). Thermo-emf of longitudinal Seebeck effect in anisotropic material is given in equation (2.6). [20]

$$U_{\mathrm{th}} = (S_{\parallel}\cos^2\alpha + S_{\perp}\sin^2\alpha)\Delta T \tag{2.6}$$

As like transverse Seebeck effect, heat and thermoelectric quantities are also perpendicular in transverse Peltier effect. While current density J is applied to anisotropic material to x-

direction, the transverse Peltier effect creates heat flux to z-direction, which gives equation (2.7). [18]

$$q'' = J * \Pi_{\mathrm{tP}} \tag{2.7}$$

where the q'' is the heat flux generated by current density J and the materials Peltier coefficient Π_{tp}. [16]

An artificially anisotropic material can be made from almost any metal, but when combining two thermoelectrically similar metals the result is quite poor as also in thermocouples. Studies of artificially anisotropic materials have been concentrated on founding good pair of materials and right angle for maximize transverse thermoelectric effect. Some examples for used materials in together are aluminum-silicon, copper-constantan, bismuth-bismuth telluride. It is proposed that artificially anisotropic material should be combination of metal and semiconductor because a semiconductor would have a large Seebeck coefficient and moderate electrical and thermal conductivities while the metal would have a small Seebeck coefficient and large electrical and thermal conductivities [12].

Intrinsic anisotropic materials are need to grow to a single crystal and have molecular structure which enables the anisotropic structure. Element like bismuth [21] and super conductors like $YBa_2Cu_3O_{7-\delta}$ (YBCO) and $Bi_2Sr_2CaCu_2O_8$ (BSCCO) [22] [23.] are examples of intrinsic anisotropic materials. YBCO –film started transverse Seebeck effect of superconductor studies in 90's and was reported to have thermopile effect in material. Intrinsic anisotropic materials have faster response times compared to thermopiles. the response time of a single crystal bismuth reaches about 9 ns in step response [21] and the response time for the YBCO -film was reported to be 1.5 ns, depending on thickness of the film. [22] BSCCO –film has also similar performance but larger Seebeck coefficient. [23]

2.3 Electric theory

In theory, electricity is electromagnetic wave travelling via a transmission path like copper wires to its destination, while current and voltage are just result of it. Electric power is transferred through in an insulator where electric and magnetic fields exist. In addition if any kind of electricity is wanted to be transferred, both magnetic and electric field should be present. [26] If electricity is a wave, then it can escape from its transmission path and interference with other circuits. The understanding of electromagnetism is based on Maxwell equations which explain both electrical and magnetic phenomena. The fundamental laws of electromagnetism are compiled to the Maxwell equations [24].

Biot and Savart's law tells that when electric current *I* is applied to conductor, it creates a magnetic field around it. Integral of magnetic field's intensity in a closed loop is equal to the current.[26] Based on this, Ampère's circuital law gives the integrated magnetic flux density ***B*** around a closed loop, where current is applied. The opposite reaction is created by Faraday's induction law, where changing flux ***B*** creates rotation of electric field ***E***. By comparing these laws, result is that, if current in one closed loop changes it induces voltage to another closed loop near the first loop. [24] This basic theory for electromagnetic generator. One can define practical solution for induced voltage when magnetic flux density fluctuates through loop area *A* [25]. When magnetic flux passes through a conducting loop, it induces voltage proportional to the flux density, the loop area and the frequency. Induced voltage can be calculated by equation (2.8). [27]

$$V_{\mathrm{n,B}} = -2\pi f B A \cos\theta \tag{2.8}$$

Where f is the frequency of the magnetic flux and θ is its phase. Flux density B needs to have a component which is perpendicular towards the loop's area A. Thus, to avoid induced noise voltage, the circuit area should be minimized and circuit should positioned way that it is along the flux. The peak value of induced voltage is absolute value of equation (2.8) when $\cos\theta = 1$.

Inductance is the property which describes the device's ability to preserve energy to magnetic field, which can see as risen voltage as inductance resists current changes. Current in inductor creates magnetic flux Φ which is product of inductance L and current i:

$$\Phi = Li \tag{2.9}$$

Equation for inductance can be generalized from the flux equation (2.9) and magnetic field resistance, reluctance. [28]

$$R_{\mathrm{m}} = \frac{Ni}{\Phi} = \frac{l}{\mu A} \tag{2.10}$$

Where l is the length of magnetic circuit and N amount of turns in a inductor and A is the area of the inductor's turns. Thus, with the equations (2.9) and (2.10) can be derived the general equation for inductance and it can be present as:

$$L = \frac{\mu A}{l} N \tag{2.11}$$

As can be seen from the equation (2.11), the inductance is related to the permeability of the surroundings and the dimensions of the inductor.

Magnetic field can create unwanted noise to other systems. When two inductors share the same magnetic field they combine a mutual inductance. In practice this means that every conductor has mutual inductance between each other's, but distance and materials between the conductors, decrements the mutual inductance which creates a series voltage source to receiving circuit which is proportional to interfering circuit's current and the mutual inductance. Figure 2.5 illustrates the equivalent circuit of inductive coupling of electromagnetic interference (EMI).

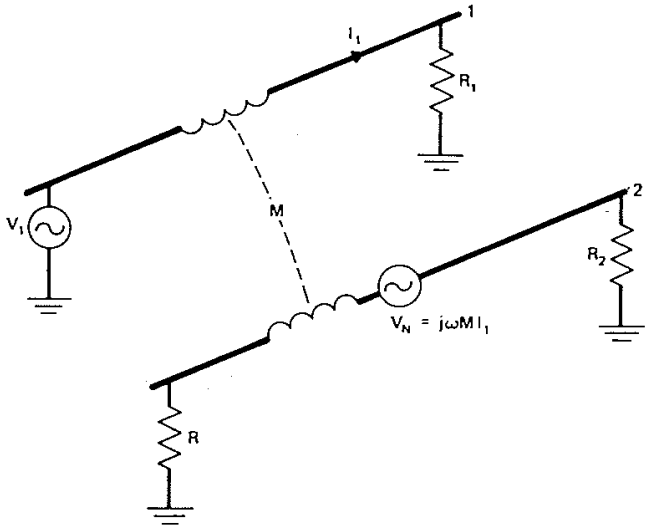

Figure 2.5 Equivalent circuit of inductive coupling. [27]

Figure 2.5 shows that inductive coupling transforms energy via magnetic field to the receiving circuit. To protect from inductive coupling, the circuit should be shielded where shield absorbs the EMI. The receiving circuit should be made less inductive by changing the dimensions of the circuit and increasing the impedance of the loop.

When magnetic field is applied to conductive material it creates opposing currents inside of the material, known as eddy currents. The opposing fields of eddy currents screens external magnetic field and strength of the magnetic field decreases logarithmically when depth of the material rises. This is called skin effect. Characteristic decay length or skin length is presented in (2.12)

$$\delta = \sqrt{\frac{2}{2\pi f \mu \sigma}}. \tag{2.12}$$

Where f is frequency of the magnetic field, μ is permeability of the material and σ is conductivity of the material. Skin depth (2.12) tells the point where magnetic flux density B is dropped 63 % from initial state. [28] Skin depth also determines the depth of current flowing in a wire with respect to the frequency f.

A capacitor is a device which preserves energy on electric field. Electric field is created between two conducting plate or between wires with different charge. Therefore, every device has stray capacitance between each others. Capacitance is affected by permittivity of material between conductors, the area and the length of the conductors.

Since there is no junction between the plates, a DC is not able to pass through a capacitor. in higher frequency current is able to bypass the capacitor which is seen as impedance. Displacement current allows the current pass through a capacitor when the frequency of the current is not DC. Therefore, capacitive coupling can occur because wiring has mutual capacitance between each other. In figure 2.6 can be seen the capacitive connections of two wires.

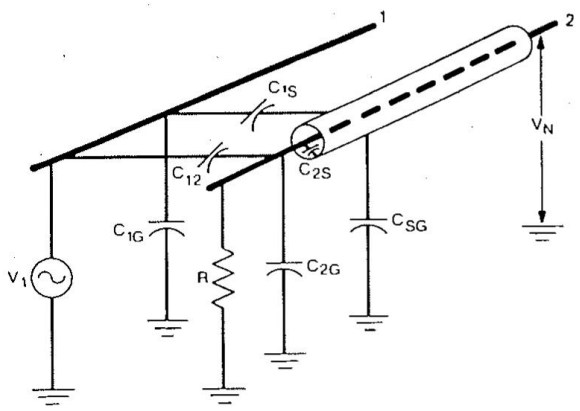

Figure 2.6 Equivalent circuit of capacitive coupling. [27]

As seen in figure 2.6, the interfering circuits voltage source can interferes the receiving circuits via more than one path and it's seen at the point $V_{n,C}$.

Inductive and capacitive coupling can be presented as an additional voltage or current sources in the receiving circuit. In figure 2.7 is presented both close field coupling methods as sources in the circuit, which receives EMI.

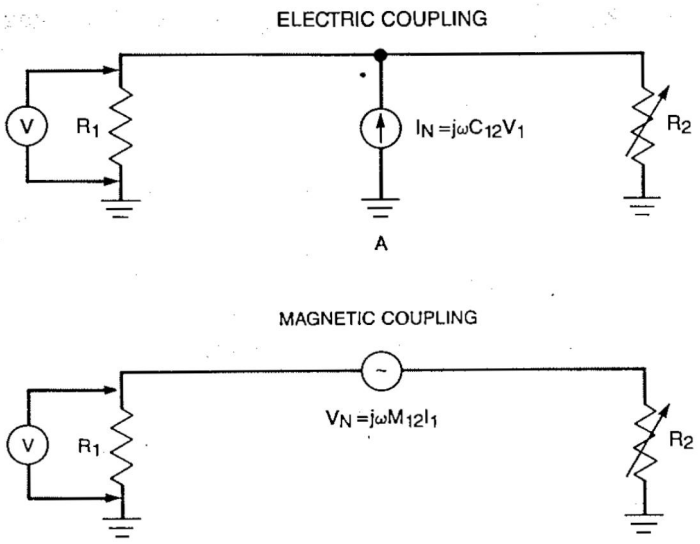

Figure 2.7 Noise sources in interfered circuit. [27]

As previous figure shows that capacitive coupling creates a parallel current source. In a differential input device, this is often referred as a common mode noise source. The current source of the capacitive coupling can be also replaced with a voltage source and the capacitance between circuits.

When a transmission line for electric wave is considered as short, all the current is on the transmission line in phase. It is then called be at low frequency region. If transmission line is long as quarter of the wavelength λ or longer, the current starts to go out of phase, then the transmission line is in standing wave region where reflections may be effected and the line is considered electrically long. [27] If one is willing to apply circuit theory, the circuit and transmission line should be in close field and keep the distances short. The limit for the low frequency region is $\lambda/10$ of the highest frequency of desired bandwidth [27]

2.4 Amplifier

Amplifier is a device which amplifies or multiplies the signal with the gain of the amplifier. Thus amplifier is a basic element in analog signal conditioning. Amplifiers can be made with a single bipolar junction- or field effect transistor but usually it needs a bias circuit for input. Operational amplifiers are multistage amplifiers implemented in a single IC. Operational amplifiers are also used as active part of filters and using right type of amplifier topology is important in signal conditioning when amplifying µV and mV level signals. Following part tells about different types amplifier circuits made with operational amplifiers. One could always implement such amplifiers from discrete transistors. This is very handy implementation when speed or other attributes need to be optimized. Unfortunately,

to work properly, the discrete transistor implementation requires also compensation circuits which include in well-designed operational amplifiers. Operational amplifiers are developed to meet all kind of requirements for many applications, which is why amplifiers made from discrete transistors are passed in this thesis. First under discussion is amplifier frontend which is the first part of the amplifier where the sensor is connected.

2.5 Amplifier frontend

Passive filter at the input is needed to decrease high frequency conducted EMI, which could get rectified in the amplifier and be seen in the output as DC. Radio frequency interference (RFI) is known to be rectified in semiconductor devices [29] and will be seen at the output of an amplifier, which means a suitable passive filter is needed to implement to front of the amplifier.

Mainly RFI noise has two types of coupling path; radiation and conduction. [29] Radiated emission can be blocked with shielding the circuit, but conductive RF emission needs to be filtered. Input filter of an amplifier needs to be passive to prevent from rectification effect. RFI-filter, in differential input is implemented with two resistors and three capacitors. Differential RFI-filter, illustrated in figure 2.8, filters both differential mode and common mode noise of input.

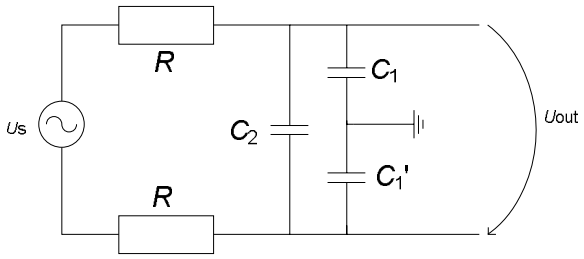

Figure 2.8 Differential RFI suppression circuit.

The common mode - and the differential signal have their own bandwidths. Resistors in figure 2.8 are mutual for both types of signals. For common mode signals capacitors C_1 and C_1' only affects to it because there is no voltage difference over capacitor C_2 for common mode voltage. Therefore common mode filter frequency can be calculated with equation (2.13), where $C_1 = C_1$'.

$$f = \frac{1}{2\pi R C_1} \tag{2.13}$$

Differential mode signals are affected all capacitors because capacitors C_1 and C_1' are in series to each other and parallel with capacitor C_2. While capacitors are in series, their combined value is half if the capacitors C_1 and C_1' are same. The equation for cut off frequency for differential filtering is in equation (2.14)

$$f = \frac{1}{2\pi R(2C_1+C_2)} \tag{2.14}$$

It is recommended to define differential bandwidth of the filter as 10 times larger than highest signal frequency to prevent attenuation of the signal. [29]

The inputs of operational amplifiers needs DC path for bias current. Usually the negative input (V-) of the operational amplifier is connected via feedback circuit to output of the operational amplifier. The bias current for the negative input is provided by that way. In non-inverting amplifier, the source is connected to the non-inverting input (V+). If only the alternating current (AC) signal is wanted to amplify, the bias current might be blocked by for example an AC coupling capacitor, and then the bias current should be provided externally. In some amplifiers have the bias bath is provided by the feedback circuits, but some may not have feedback in inputs and so it doesn't have the bias path if it has a floating source like an active sensor. One way is to add grounded resistors directly to both inputs. Practically the source is still floating, but bias current is able to travel to amplifiers input. [30] [31] However, the mismatch of the resistors caused by inaccuracy decreases the common mode rejection ratio (CMRR). One could solve this by using precision resistors. Unfortunately this can be very costly decision. The need of accurate resistors is decreased when bias resistors are connected to ground via mutual resistor. [32] Both circuits are presented in figure 2.9. By choosing a larger resistor for the grounded resistor than parallel resistors, the mismatch effect is damped, even when using 1 % or 5 % accurate resistors.

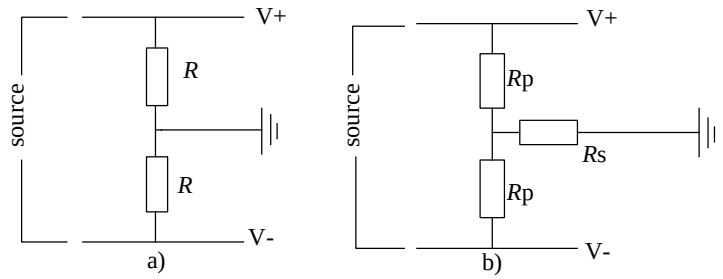

Figure 2.9 Bias resistor circuits a) two parallel b) two parallel and one series resistor. Circuits have a differential source and they are connected between inputs of an amplifier V+ and V-.

Higher symmetry of resistors is gained with the b) case of figure 2.9 when series resistor R_s is relatively larger than parallel resistors which are marked as R_p at figure 2.9 b). Unfortunately parallel resistors are also in parallel with amplifiers input resistance, which means that the total input resistance decreases. The parallel resistors decrease the ground impedance for common mode voltage which gives lowers the CMRR. Also one need to take care that minimum bias current is available for amplifier. Johnson noise created by bias resistors in differential input amplifier, connects to amplifier as common mode noise source. Common mode rejection of the amplifiers helps in ideal case but other part of the input circuit makes for these noise sources unsymmetrical and generates noise to input. RFI filter's capacitors on the other hand form a low pass filter with a bias resistor.

2.6 Amplifier topologies

Amplifier circuits can be four types: voltage, current, trans-impedance or trans-conductance amplifiers. The transverse Seebeck effect is a voltage source and that's the obvious reason for using a voltage amplifier. In this part voltage amplifier topologies are presented. The amplifier topologies are circuits implemented with operational amplifiers. Everything listed below are single ended output amplifier but they also have differential output versions if the output of the operational amplifier is fully differential.

2.6.1 Single ended input amplifiers

A single-ended input amplifier is the basic amplifiers implemented by operational amplifiers. The operational amplifier can be inverting or non-inverting. Circuits for both of them are presented in figure 2.10. The closed loop gain of the amplifier is set by two external resistors where equation (2.15) is for non-inverting amplifier.

$$G_{\mathrm{cl}} = 1 + \frac{R_{\mathrm{f}}}{R_{\mathrm{in}}} \tag{2.15}$$

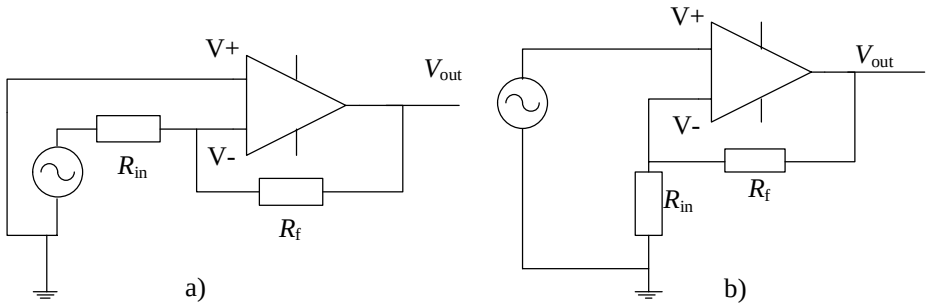

Figure 2.10 Single-ended amplifier topologies a) an inverting amplifier b) a non-inverting amplifier

Input impedance of the single ended operational amplifier is set by external resistor which determinate the gain of the amplifier in inverting amplifier. A non-inverting amplifier's input impedance is directly the input impedance of operational amplifiers input impedance. [30] [31] In figure 2.10 the resistor R_{in} determinates the input impedance of an inverting amplifier .Therefore a large resistor is needed to achieve high impedance. Large resistors have large thermal noise which increases the output noise.

CMRR is poor in case of an inverting amplifier. The input is directly connected to the output, with feedback resistor R_f. While the common mode voltage is present and an operational amplifier amplifies only the voltage difference between inputs. Then the common mode voltage has unity gain at the output which gives CMRR of 0 dB. [29]

2.6.2 Differential amplifier

Sometimes it is needed to amplify voltage difference but the input cannot be grounded. Measuring with a current shunt is usually that kind of an application which needs A differential input amplifier. A differential amplifier is a single operational amplifier circuit with four resistors. Circuit of a differential amplifier is presented in figure 2.11 and the equation for the output voltage is in (2.16).

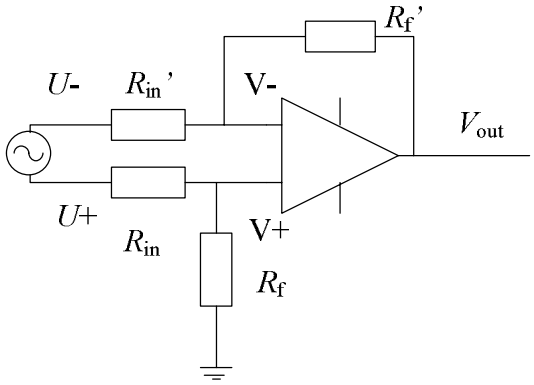

Figure 2.11 Circuit of differential amplifier, where $R_f = R_f$' and $R_{in} = R_f$'.

$$V_{out} = (U_+ - U_-)\frac{R_f}{R_{in}} \tag{2.16}$$

Where V_{out} is the output voltage of the amplifier and U_+ and U_- are the input voltages, and R_f, R_f', R_{in} and R_f' are feedback resistors. Differential amplifier also suffers the input impedance weakness like the inverting single ended input amplifier. The input impedance is set by input resistors. The input pins of the operational amplifiers have 0 V of voltage difference, thus the input impedance $Z_{in} = R_f + R_f$'. [30] the common mode rejection ratio is far better because the sensor is no longer connected to ground. One advantage of this circuit is that input pins of the operational amplifiers have DC current path for input bias cur-

rent vie feedback resistors. In the ideal case CMRR is infinite, but the resistors have to be matched well to achieve high CMRR. In fact the maximum CMRR for a differential amplifier, made with one operational amplifier, is presented in (2.17).[33]

$$CMRR = \frac{G+1}{4t} \tag{2.17}$$

where *G* is differential gain of the amplifier and *t* is the tolerance of resistors. In addition to that there is also the *CMRR* of the operational amplifiers. These are summed together as parallel [33]. Therefore, *CMRR* is in a real case always lower than CMRR made by resistors (2.15). Single-ended output differential amplifiers can be analyzed as inverting amplifier, which has a grounded voltage divider at the non-inverting input.

2.6.3 Intsrumentation amplifier

Another differential input amplifier is an instrumentation amplifier. It has more complex structure than topologies above, but its both inputs have high impedance and may not require any resistor that could affect the input impedance of the amplifier. In figure (2.12) is the circuit of a classic topology of an instrumentation amplifier. [29]

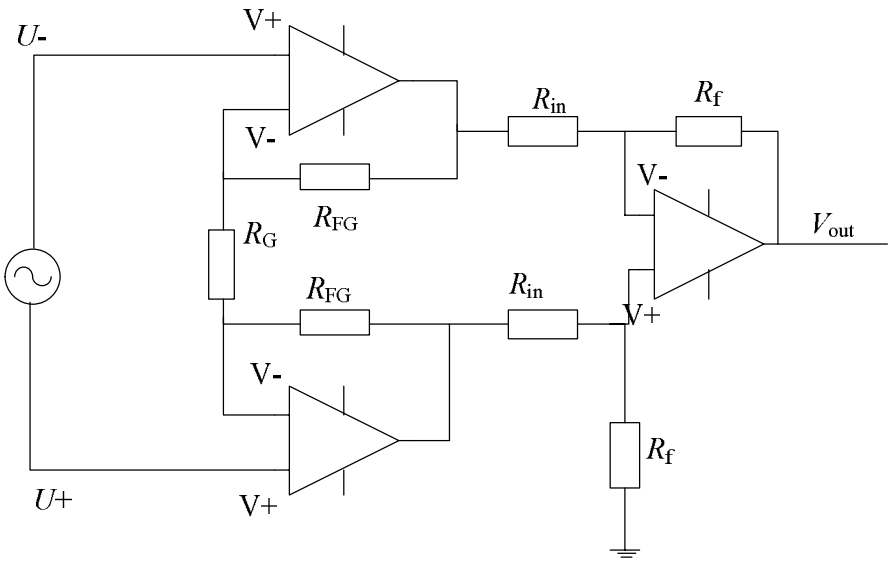

Figure 2.12 Classic topology of instrumentation amplifier with three operational amplifier. The amplifier can be sectioned to the input stage and the output stage. The input stage consists of two non-inverting amplifier, which are connected to the source. and the single differential amplifier is the output stage.

Instrumentation amplifier is also an operational amplifier based amplifier. It consists of three or two operational amplifiers. Two non inverting operational amplifiers form the in-

put stage of an instrumentation amplifier. [29] Output stage is a differential amplifier which determines which of the inputs are inverting or non-inverting. Instrumentation amplifier has great input impedance since its input is directly connected to the high impedance non-inverting inputs of the operational amplifiers. Also the CMRR is optimized and the higher the gain of the input stage the higher is the CMRR [33]. Although the input bias current path should be provided for the input, but that could affect the CMRR.

As mentioned, the input stage is formed by two non-inverting amplifiers. They both share one resistor which defines the amplification of both amplifiers. Output stage's amplification is same with a differential amplifier which is stated in equation (2.16). Combined amplification of these is presented in equation (2.18). [30] [31]

$$V_{\text{out}} = (1 + \frac{2R_{\text{FG}}}{R_{\text{G}}})(U_{+} - U_{-})\frac{R_{\text{f}}}{R_{\text{in}}} \tag{2.18}$$

Where V_{out} is the output voltage of the amplifier and U_{+} and U_{-} are the input voltages, and R_{f}, R_{in}, R_{FG} and R_{G} are feedback resistors. [30] [31] Instrumentation amplifiers are produced as single chip products where some of the feedback resistors are embedded within to the amplifier IC. The advantage for this is gain accuracy and high matched resistor to achieve high CMRR. Resistor R_{G} is usually left out from the IC because, the gain can be set externally. There is also fixed gain amplifiers where the R_{G} is integrated to the IC.

Usually manufactures implement the output stage of the instrumentation amplifier with unity gain. In that case all the amplification is applied in the input stage. This will surely decrease the bandwidth of the input stage, hence it affect to whole amplifiers bandwidth too. Sometimes it would be needed to design an instrumentation amplifier from operational amplifiers to reach the desired gain and bandwidth

2.7 Non-idealities of amplifiers

Theoretic amplifiers have infinite high input impedance and infinite low output impedance and often this assumption can be used, but in practice values are not infinitely high or low and in addition to a real amplifier, the design affects to these values. There are other non-idealities too, but first some theory behind them is discussed next.

2.7.1 Other phenomena related to temperature in electronics

These are not signed as thermoelectric phenomena, but they are worth mentioning in this master thesis. The phenomena listed below are related to electronics and they are proportional to the operating temperature of electric components.

At the start of this chapter joule heating was mentioned. When current is applied through a resistance it chances the electrical energy to thermal energy which result is voltage drop. This means that the component's temperature rises if its heat is not properly transferred. The heating power comes from the Ohm's law, which is product voltage and current. The Joule heating is common source of heat in electronic devices and should be taken care especially in linear regulator design where regulated voltage is generated with decreasing the input voltage to desired output voltage by *IR* loss. Temperature rise is ruled by the ambient temperature of a device and thermal conductivity and other heat transfer parameters.

2.7.2 Johnson-Nyquist noise

Johnson noise (or Johnson-Nyquist noise) is noise in a conductor generated by thermal movement of molecules. Johnson found the relationship of the noise density and temperature and published his discovery in 1921. [34] The root mean square voltage of Johnson noise to given bandwidth is presented in equation (2.19)

$$\overline{V^2} = 4\mathrm{k}TR\Delta f \tag{2.19}$$

As we can see from equation (2.17 the noise is proportional to resistance of the material from which can be deduce that larger resistors are noisier. Therefore, using too large resistor is not good thing if the noise is critical value of the system. An equivalent circuit for a resistor with Johnson noise source is presented in figure 2.13. The thermal noise source is in series with the resistor. [15]

Figure 2.13 A resistor with thermal noise source or Johnson noise.

The equation of (2.19) simplifies to equation (2.20) of spectral noise density. Which unit is $\frac{\mathrm{V}}{\sqrt{\mathrm{Hz}}}$ but more often $\frac{\mathrm{nV}}{\sqrt{\mathrm{Hz}}}$ is used due the smallness of the value. [15]

$$V = \sqrt{4kTR} \tag{2.20}$$

Johnson noise should be noticed when designing amplifier for low level sensors with large gain.

2.7.3 PN-junction current law

Common connections in semiconductor devices are PN-junctions which are formed when a P- and an N- type semiconductor are connected together. This forms the most basic semiconductor device, the diode, but it appears in many other semiconductor devices like bipolar junction transistors. Diodes have a property which allows pass current in one direction. PN junction creates potential gap known as threshold voltage which is needed over pass to let current through the PN-junction. This threshold voltage relates on applied-current and temperature. This is named as current law of PN-junction. The rising temperature increases the current through the PN-junction. In case of constant current, the effect can be seen as decrementing of the threshold voltage of PN-junction. PN-junction current law is one of the reasons of non-linearity of semiconductor devices, when temperature changes.

2.7.4 The model of operational amplifier

All the temperature related phenomena presented above, appears in semiconductor operational amplifiers. But there are more non-idealities in operational amplifiers and they are related other parameters too, like electrical properties and dimension. As some to mention, operational amplifiers have parasitic capacitance at inputs and limited current supply at output. Inputs of operational amplifiers must provide a DC-path for bias current to keep the amplifier operative. Operational amplifiers have even more performance limiting properties that must take care of when designing an amplifier. Figure 2.14 presents a model of a non-ideal operational amplifier.

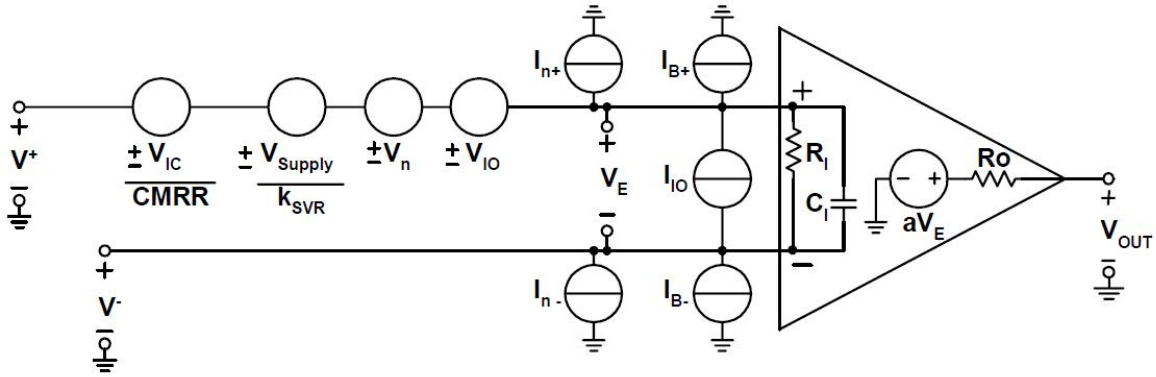

Figure 2.14 A model of non-ideal amplifier. [35]

From figure 2.14 can be seen that various things affects to the input of the amplifier. Not all variables are interested in this thesis. Significant on figure 2.14 is to notice that operational amplifier has limited input resistance and parallel input capacitance. There are also input bias currents for inputs of the operational amplifier and input offset V_{IO} and input noise V_n as differential voltage error sources.

A non-ideal operational amplifier can be modeled to be first order system. Operational amplifiers have limited gain and it is proportional to output frequency. The open loop gain limits amplifier to work on intended gain which comes from the feedback loop. For example, the equation for non-inverting amplifier (2.15) is true with ideal amplifiers. In the real world nothing is ideal, the gain of a real operational amplifier is limited and the feedback circuit decreases the output gain or the closed loop gain (G_{cl}). The limiting factor is the open loop gain of the amplifier (G_{ol}). Operational amplifiers can be descripted by single pole system with a transfer function given in equation (2.21). [36]

$$|G_{\mathrm{cl}}(f)|_{\mathrm{dB}} = 20\log\frac{\frac{G_{\mathrm{ol}}}{1+\beta G_{\mathrm{ol}}}}{\sqrt{1+\left(\frac{f}{f_0}\right)^2\frac{1}{(1+\beta G_{\mathrm{ol}})^2}}} \tag{2.21}$$

if frequency it at DC then equations simplifies to

$$|G_{\mathrm{cl}}(f = \mathrm{DC})|_{\mathrm{dB}} = 20\log\left(\frac{G_{\mathrm{ol}}}{1+\beta G_{\mathrm{ol}}}\right). \tag{2.22}$$

Where β is the feedback gain, defined by the resistors. [36] When investigating the equation (2.22) can be see that, if the feedback gain is larger it affects to the closed loop gain of the amplifier. Therefore, a higher open loop gain provides better DC gain accuracy.

A requirement for working properly is that operational amplifiers' input stage transistors needs bias current. The amount of current needed depends on the design of the operational amplifier as well the input stage transistor types, whether are they bipolar junction transistors or junction field effect transistor.

2.7.5 Ambient of the electronics

When heat flux is measured, there is always temperature difference present. This can affect also to the amplifying circuit. Heat can affect to every part of the circuit. Rising temperature not only brings noise but also it changes many values in semiconductors and other components, including resistors and capacitors. If temperature rises over the components operating temperature, the component is no more at specified value and can be permanently damaged or destroyed. Components have also lowest operating point.

Adding an amplifier near to a sensor decreases the parasitic components of a sensor cable and EMI coupling to the signal. When heat flux is measured the ambient temperature can difference very widely and it may affect to the amplifier. Since the output voltages of heat

flux sensors are relatively small, therefore gain should be high. All amplifiers have voltage offset at their input and also at the output. The input offset voltage is generated by input bias currents of the input stages. The differential stage at the amplifiers input has transistors. At the end these transistors are always somehow unique so they draw different amount bias current which generates the input offset voltage. [15] If the input offset V_{OSI} is high (100 µV … 1 mV or more) the amplifier loses its input range and may even saturate the output. A constant input offset can be live with because it can be calculated out from the measurement result if temperature is constant. The more important parameter for amplifier is the input temperature drift coefficient. Temperature drift in the input changes the offset voltage V_{OSI} proportional to the temperature of the amplifier. For BJT input operational amplifiers, PN-junction current law is one cause for the drift. If the amplifier has a large input temperature drift coefficient it is could affect the output of the amplifier without acknowledging the error. The mentioned output saturation is possible to happen. For example the amplifier has output range ± 5 V and the input offset voltage is at room temperature 100 µV and the temperature drift of the input is 10 µV/^{0}C. The gain is set to 1000. The temperature then raises 75 degrees. Now we can see 850 mV at the output with zero input. The output didn't saturated yet but 17 % of the positive input voltage range has been lost. In the worst case, drifting could be left totally unnoticed and the change of input offset voltage is counted as result of a measurement.

2.8 Amplifiers used in thermoelectric study

There are a few amplifiers for the heat flux measuring in the market. Vatell Corporation and Hukseflux provide both sensors and amplifiers to heat flux metering, although sensors are based on thermopile technology. Both companies provide battery powered amplifiers. Hukseflux AC100 and NAM01 have high gain, up to 1000 and 10000, respectively. Hukseflux LI19 is a hand held data logger with a resolution from 1 to 10 µV. All these amplifiers have response time of 1 s.

Vatell Corporation provides amplifiers with variable gain set. For example AMP6 has gain from 1 to 5000 with 1 MHz and 5 kHz bandwidths respectively. Amplifiers have also high input impedance and accuracy from 0.6 to 3.6 % depending on the gain selected. Sujay Raphael-Mabel used AMP6 amplifier in his Master's Thesis, in which he design a high temperature thermopile heat flux sensor [5].

Both manufactures doesn't reveal the circuits of the amplifier but it seems that the amplifiers are implemented with instrumentation amplifiers. Since the gain of Hukseflux's AC100 is set by a single resistor. From the high input impedance of a Vatell AMP6 can be deduced, that it is based on an instrumentation amplifier.

Ewing did Master's Thesis [37] in Virginia Polytechnic Institute about a direct measurement thin-film heat flux array. This thermocouple based heat flux array had instrumentation amplifiers as a front end amplifier for data acquisition device. The instrumentation amplifier use was Analog Devices AD624. The selection criteria for the amplifiers were capability to have gain as 1000 and a relatively small noise specification on low frequencies. Also the high CMRR was noted to be a reason to choose the specific amplifier.

Mann used National Instrument's SCC-AI series signal conditioning modules in his Master Thesis [12], which have instrumentation amplifier, a low pass filter and isolation and at least 1 MΩ input impedance. These are parts for modular instrumentation system for data acquisition (DAQ). SCC-AI amplifier modules have bandwidth from 4 Hz to 10 kHz. Modules input voltage span are from ±100 µV to 42 V.

The desired properties for amplifier circuits are small input capacitance and high input resistance. The input offset should be low as possible but more important parameter is temperature stability. While the amplifiers on the market and amplifiers made for other researches it is convinced to use instrumentation amplifiers or at least differential amplifiers on thermoelectric applications. It is deduced from the studies that even at laboratory conditions, differential input amplifiers should be used.

3 INSTRUMENTATION OF TRANSVERSE SEEBECK EFFECT SENSORS

Heat flux sensors based on thermoelectric effects and the sensor used in this case are introduced and studied in this chapter. Traditional thermoelectric sensor for heat flux measurement are thermopiles which are multiple thermocouples piled together. Thermocouple junctions have thermal barrier to create needed temperature difference between the junctions. When hundreds or even thousands thermocouples are implemented to a one thermopile, the internal resistance of the thermocouple could rise quite high, from hundreds to thousands ohms. Therefore, response time is quite slow due the high resistance and the thermal insulator. Heat flux sensing with thermopiles is based on Fourier's law (1.1) where temperature difference create voltage to thermocouples of the thermopile.

Thermopiles are widely commercially available in many shapes and size. Also thermopiles can be implemented various ways from block construction to wire wound and even micro electro mechanical systems are studied.[4][38]

3.1 Heat flux sensors based on transverse Seebeck effect

Heat flux sensors based on transverse Seebeck effect are not so widely developed as traditional thermopile sensor. Sensors based on transverse Seebeck effect are faster than thermopile sensor because their output voltage is proportional to temperature gradient instead of exact temperature of junction of the thermopile. [22] Here is a short review about studies and products, which are using transverse Seebeck effect for heat flux sensing. Some of the listed sensors are still on an experimental level.

Mityakov et al have been produced several types of heat flux sensors based on intrisitic anisotropic single crystal bismuth called a gradient heat flux sensor and multilayered artificially anisotropic materials. [21]

Fortech HTS GmbH. produces YBCO film based commercially available atomic layer thermopile (ALTP) heat flux sensors. The sensors are based on transverse Seebeck effect although they are named ALTP. Company reports that the sensor is capable to 300 kHz…1 MHz bandwidth, which is limited by the coating layer on YBCO film. [39]

Sujay Raphael-Mabel made his Master's Thesis about a high temperature heat flux sensor from brass and steel. He tried to construct transverse Seebeck effect sensor same way like a GHFS from the materials, but after all he ended to make a thermopile sensor. [5]

Brooks Samuel Mann studied cooling and heat flux sensing properties of artificial anisotropic material made from bismuth-telluride and bismuth. The heat flux sensing property was found more promising than cooling. [12]

Derryberry studied n-type bismuth telluride and titanium grade 5 based transverse Seebeck effect sensor. The result was that the output voltage was enlarged when material structure approached near 45 degrees. The output is also proportional to the length of the sensor. Time response is affected by the thickness of the sensor and the bonding of the material layers. Highest Seebeck coefficient of the sensor, with 59 degrees material angle, was tested to be 640 µV/K. [10]

Kyarad studied transverse Seebeck effect sensing with artificially anisotropic materials made from chrome-constantan and aluminum-silicon. It was found, that the anisotropic aluminum-silicon material had Seebeck coefficient of 1.5 mV/K. The time response was reported to be near the response time of the testing laser. [20]

3.1.1 Gradient heat flux sensor

For further study in this thesis, gradient heat flux sensors (GHFS) were available which are based on transverse Seebeck effect. In the case, there was also two GHFS placed in the air gap of the motor. These sensors are based on anisotropic thermo-elements (AT) made from single crystal bismuth which is intrinsically anisotropic material. Bismuth ATs are cut from bismuth crystal in direction along crystallographic axels, so the ATs become anisotropic and enable transverse Seebeck effect. ATs are assembled in series to create larger thermo-emf to output. In 3.1 the sensor and its parts are illustrated. [21]

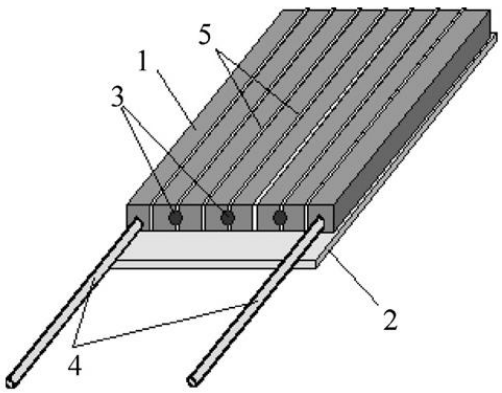

Figure 3.1 Construction of a Gradient Heat Flux Sensor. GHFS consists of next pieces 1: Bismuth anisotropic thermo-element, 2: Thermal washer, 3: ATE junction soldering; 4: Connection wires. [21]

Due the melting point of bismuth the maximum temperature of the sensor is 271 ^{o}C. Output voltage and other properties of the sensor is scientifically studied [21]. The output voltage equation is based on Seebeck coefficient of the bismuth AT from which can be calculate the output voltage U_{GHFS} of the sensor generated by heat flux is

$$U_{\mathrm{GHFS}} = S_0 * q_z'' * A \tag{3.1}$$

Where A is the area of the sensor, S_0 is the sensitivity and q'' measured heat flux. [21]

GHFS's output dynamic properties and response to heat flux is studied. The sensitivity S_0 of the sensors used in our case is 10 mV/W and the area is 0.0001 m^2. The time constant for a GHFS is reported to be about 9 ns [21], which is bandwidth of 17.7 MHz. The response time was calculated from a signal from where the actual steady state of the signal is not observable. The steady state of the signal should be the reference level for the time constant. Instead of the steady state, the time constant was calculated from the highest peak of the time response which time was 14.2 ns. If this is the fastest response of the sensor, then 1/(14.2 ns) yields the bandwidth of 70.4 MHz. With the same way were calculated time constants for YBCO and BSCCO films. Their time constants were calculated from the highest peak of the step response. Nevertheless the reported time constants and bandwidths are used in this thesis.

3.2 Loading of transverse Seebeck effect sensors

To find a proper way to measure a transverse Seebeck heat flux sensor, the loading effect should be known. This means that what does the characteristic of the sensor's load to output signal. Therefore, an equivalent circuit of the sensor should be studied. Transverse Seebeck effect sensors are self generating and measured quantity is voltage. Other sensors based on transverse Seebeck effect were not available than a GHFS, but it can be assumed that the study methods and results should be applicable to others as well. However, the study is made with a GHFS, which has different structural than others, but nevertheless the principle is same. It is possible to construct sensors same way like the GHFS, with different materials.

The output voltage of a GHFS is generated by thermo-emf of ATs. Since there are multiple thermoelectric voltage generators in series, then Thevenin's equivalent source is used, so every AT has its own internal resistance. Equation (3.2) is generated from the circuit of figure 3.2, when n amount of ATs is applied in series.

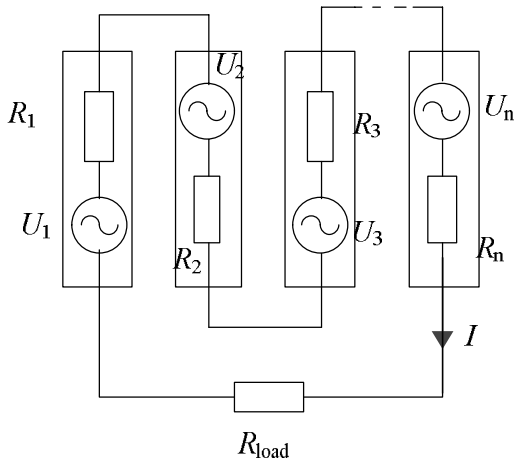

Figure 3.2 The circuit of GHFS with *n* –amount of ATs connected in series

$$U_1 - IR_1 + U_2 - IR_2 + U_3 - IR_3 + \ldots + U_\mathrm{n} - IR_\mathrm{n} - IR_\mathrm{load} = 0 \tag{3.2}$$

Then the equation (3.2) simplifies to:

$$(U_1 + U_2 + U_3 + \cdots + U_\mathrm{n}) = I(R_1 + R_2 + R_3 + \cdots + R_\mathrm{n} + R_\mathrm{load}), \tag{3.3}$$

where the term IR_{load} is same as the output voltage U_{out} and substituting term U_{out} to the previous equation (3.3) The equation simplifies to

$$(U_1 + U_2 + U_3 + \cdots + U_\mathrm{n}) = \frac{U_\mathrm{out}}{R_\mathrm{load}}(R_1 + R_2 + R_3 + \cdots + R_\mathrm{n} + R_\mathrm{load}). \tag{3.4}$$

The sum of the voltage sources can be summed and they form a term U_s which is the output signal of the sensor. Also internal resistors can be summed and they form the output impedance of the GHFS at DC. When output voltage over R_{load} is calculated, it can be deduced that resistance and voltage sources can be summed and U_{out} is result of voltage divider formed by sum of internal resistances $R_{internal}$ and R_{load}. Thus the equation of the output voltage:

$$U_\mathrm{out} = \frac{R_\mathrm{load}}{R_\mathrm{load} + R_\mathrm{internal}} U_\mathrm{s} \tag{3.5}$$

From the equation (3.5), an assumption can be made that the load for the sensor needs to be as high impedance as possible. Since the sensor is a voltage source, its output impedance divides the output voltage with load impedance. A sensor with more than one element doesn't have difference with a sensor made from one element, when considering the internal resistance and the generated voltage of the sensor.

Unfortunately, there are no purely resistive or reactive components. Every real circuit component is combination of reactive and resistive components. The GHFS is announced to have the time constant of 9 ns and YBCO film 1.5…100 ns in step response test. In that speed and full bandwidth of the sensors reactive components become observable. Parasitic capacitance and inductance are always somehow related to dimensions and surroundings of sensors. Therefore, a GHFS has also parasitic inductance and capacitance what might be proportional to a sensors platform material and insulation material. In case of a GHFS, there is capacitance between the individual ATs too.

The parasitic components affect the bandwidth of the sensor. Also there are some frequencies where inductances and capacitances resonate. Parasitic component are usually unnoticeable when frequencies are low, which depends on values of reactive components. A GHFS is capable up to 9 ns of response and YBCO films even faster. This means that at the higher frequencies parasitic components will have some effect to sensors output. To study the parasitic components of a sensor, the impedance measurement is made. For a GHFS the measurement was made with HP 4194A impedance analyzer with HP 16047D instrumentation fixture. With this four wire impedance measurement method sweep of 100 Hz to 40 MHz was supplied to the sensor, which was the maximum bandwidth of HP 4194A in impedance measuring. The sensor is attached on an aluminum plate with twisted pair wiring and it was placed in a box, while the measurement was going on, for keep the sensor in constant temperature and protect it from light to make sure that sensor won't create signals to disturb the measurement. The result of the measurement is presented in figure (3.3).

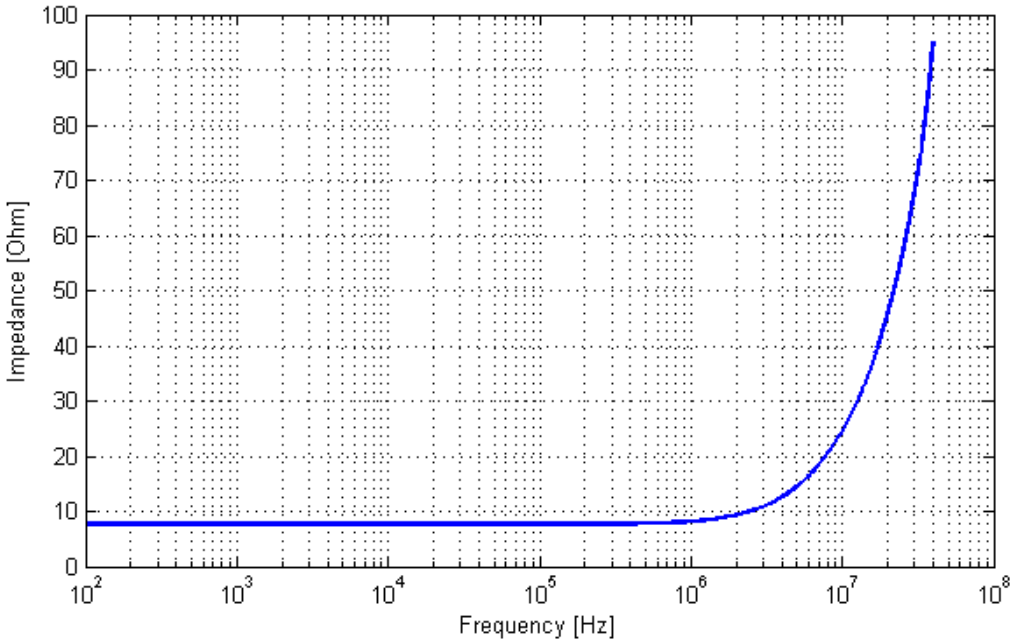

Figure 3.3 Measured absolute value impedance of a gradient heat flux sensor on an aluminum plate.

As can be seen from figure 3.3, the impedance is rising as the frequency grows from 7.63 Ω to 95.20 Ω. In this bandwidth, the resonance point is not observable. This means that dominating part of the reactive components of the sensor in this bandwidth is inductance. One should notice that the measurement includes the parasitic components of the measurement setup and wiring too, but they are assumed to be low enough that they can be left out. The rise of impedance at figure 3.3 could also be affected by skin depth in higher frequencies. Since the area of current decreases, the resistance rises because it is proportional to the area of the conductor. According to equation of the skin depth (2.12), AC resistance is not linear effect, and if impedance figure is drawn to linear frequency plot, the rise of impedance is quite linear.

Due the structure and the impedance curve of the sensor, there is also expected to be parasitic capacitance in the circuit, while the dominant part is the inductance. The sensor creates a loop with the wiring, which inductance is affected by the area of the loop and its permeability of the surroundings, according to equation (2.11). Therefore, proposed the equivalent circuit of an inductor can be applied to the sensor. Figure 3.4 shows equivalent circuit for the inductor. [40] Its components are resistance, inductance and parallel capacitance.

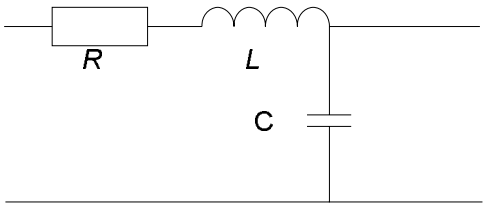

Figure 3.4 An equivalent circuit of an inductor or a cable

Transfer function for circuit in figure (3.4) is

$$H(s) = \frac{\frac{1}{LC}}{s^2+\frac{R}{L}s+\frac{1}{LC}}. \tag{3.6}$$

Where *R*, *L* and *C* are the components of the circuit in 3.4. The transverse Seebeck effect as a voltage source is added to circuit in figure 3.4, which produces a non-ideal model for GHFS. Figure 3.5 illustrates this equivalent circuit. Where the voltage source is thermo-emf created by heat flux.

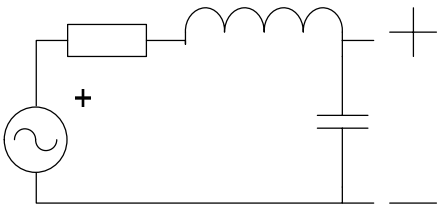

Figure 3.5 When a voltage source is added to the circuit of figure 3.4, it forms the equivalent circuit for the GHFS.

Circuit in figure (3.5) is only simplified circuit for a GHFS or another transverse Seebeck HFS. In instrumentation, there is always a signal cable and a measurement device such as an amplifier or an oscilloscope. The equivalent circuit for cable is as same with inductor if applied in the close field and the parallel conductance is ignored. [26] Figure 2.14 shows that the input of an amplifier has not infinite impedance. Input parameters for amplifiers are input resistance and input capacitance which together form the input impedance.

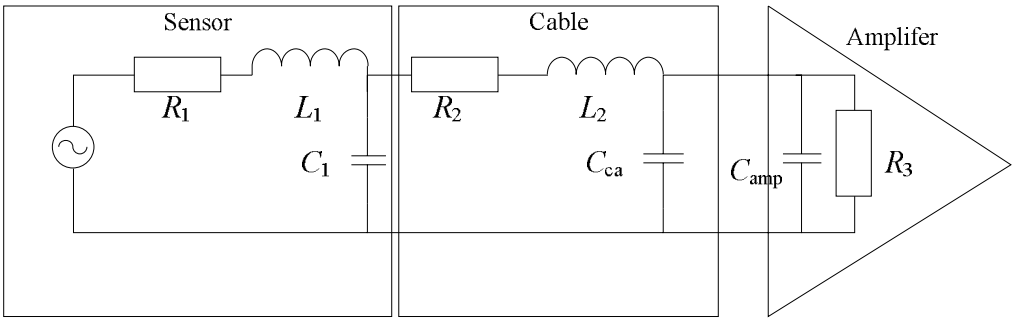

Figure 3.6 An equivalent circuit for GHFS with a cable and amplifier

When looking the circuit in figure 3.6, it is seen that the instrumentation circuit has no component that prevents DC voltage. There are also two circuits, the sensor and the cable, which could be analyzed with the transfer function in equation (3.6). The transfer function of the whole circuit of figure 3.6 is formed with Thevenin's method with two current loops. The output voltage is result of the current of amplifier input impedance, which is presented in (3.7). The calculation of the transfer function (3.7) can be seen in Appendix II.

$$\frac{U_{\mathrm{out}}(s)}{U_{\mathrm{S}}(s)} = \frac{R_3}{\begin{aligned} s^4 + s^3\left(\frac{1}{C_2R_3}+\frac{R_1}{L_1}+\frac{R_2}{L_2}\right) + s^2\left(\frac{R_2}{C_2L_2R_3}+\frac{R_1}{C_2L_1R_3}+\frac{1}{C_2L_2}+\frac{1}{C_1L_2}+\frac{1}{C_1L_1}+\frac{R_1R_2}{L_1L_2}\right)\cdots \\ + s\left(\frac{1}{C_1C_2L_1R_3}+\frac{1}{C_1C_2L_2R_3}+\frac{R_1R_2}{C_2L_1L_2R_3}+\frac{R_1}{C_1L_1L_2}+\frac{R_1}{C_2L_1L_2}+\frac{R_2}{C_1L_1L_2}\right)\cdots \\ + \frac{R_1+R_2+R_3}{C_1C_2L_1L_2R_3} \end{aligned}} \tag{3.7}$$

where R_1, L_1 and C_1 are components of the sensor, R_2 and L_2 are cable components, C_2 is sum of cable and amplifier capacitances $C_2 = (C_{ca} + C_{amp})$ and R_3 is the input resistance of the amplifier. As predicted no zeros appears in the transfer function. Therefore, the circuit is low pass type. As can be seen from equation (3.7) the wiring and the input characteristics do affect to the bandwidth of the sensor output. The parameters of the wire are proportional to the length of the cable. Therefore, the cable length should keep short as possible. Also requirement to apply circuit theory, the length of the cable should remain in close field compared to the maximum wavelength λ. Theory says $\lambda/10$, [27] but rule of thumb suggests that the length should be less than $\lambda/16$.

The capacitance of the amplifier's input is more important than the resistance. While the sensor's internal impedance is quite low compared to amplifier's input impedance. Therefore, capacitance is the main parameter to affect the bandwidth. The equivalent circuit 3.6 and the transfer function (3.7) should apply to every sensor which has inductor like structure. Therefore, it can be declare that all transverse heat flux sensor

From the equation (2.9) can be seen that inductance is proportional to surrounding permeability $\mu_0\mu_r$ of the inductor's core. In electrically gradient heat flux sensor in a construction like in figure 3.5, can be proposed to be an inductor with a core, where the core is the platform of the sensor. Effect of the parasitic components can be seen at the top of the sensors bandwidth as limiting factor and overshooting on fast transient situations.

With the impedance analyzer HP 4149A, the values of equivalent circuit in figure 3.5 can be calculated. Measurements gave firstly negative capacitance value. But after rearrangement of measuring wires realistic values was received. The analyzer calculated values for resistance 7.65 Ω, inductance 392 nH and capacitance 403 fF. After several measurements, measured capacitance varied from 400 fF to 2.5 pF depending on the wiring position, as mean value 1 pF. Conclusion of the measurement is that wiring attachment is greatly affecting the output function of the sensor. Capacitance can be also thought to be small enough to leave unnoticed since it can be deduce that the wiring of the measurement makes most of the parasitic capacitance.

For an example how the wirings affects to the whole frequency response of the circuit, when using the same assembly of the sensor and adding measurement cable between the sensor and oscilloscope which replaces amplifier in figure 3.6. Parameters for the oscilloscope are from Tektronix TDS 3502. The input resistance is 1 MΩ and the capacitance 13 pF. As parameters of the wire are used a 50 Ω coaxial cable at the maximum length for a short cable in bandwidth of 17.7 MHz which yields 1.06 m, when cable length is one sixteenth of the wave length. When using typical RG-58 cable, the parasitic components can be calculated from datasheet information provided by a manufacturer. [41]. Values of parasitic components are relative to cable length. For the 0.17 m long RG-58 coaxial cable, the parasitic component values are: R = 0.25 mΩ/m, L = 0.21 µH/m and C = 79.72 pF/m. When the values are multiplied with cable length, the values are 0.27 mΩ, 222.6 nH and 84.5 pF respectively. The measured values of the sensors parasitic components are affected by the twisted pair cable attached to the sensor. According to equation (2.11), the cable forms with the sensor the loop area which determines the inductance of sensor, but also parasitic components cable itself is included to the measurement value. That's why this frequency response calculation is for illustrative purposes only.

When using the model from figure 3.6, the equation (3.7) can be use to draw the Bode plot from the system. This tells about the frequency and phase response of sensor. When the parameters are used in the equation (3.7), the Bode plot is drawn with MATLAB. The Bode plot of the system is presented in figure 3.7.

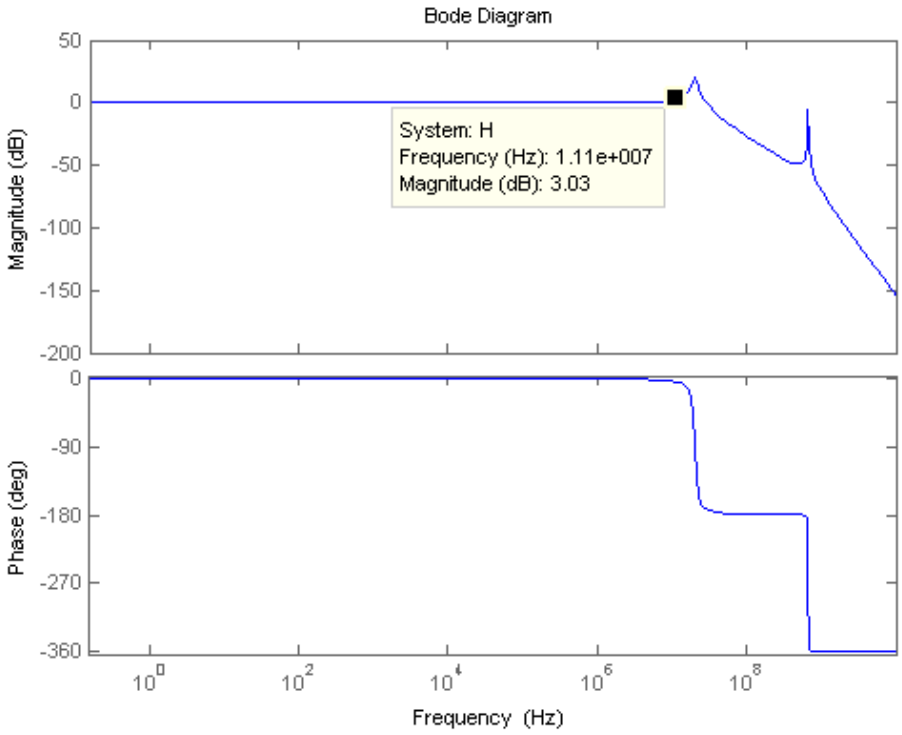

Figure 3.7 Bode plot of the system of figure 3.6 with measured and calculated values. ± 3dB bandwidth is limited to 11 MHz.

From the Bode plot in figure 3.7 can be seen two resonance points as the fourth order transfer function suggest. The Bode plot shows that first resonance frequency appears around 20 MHz which affect also to lower frequencies. The second is far away from the bandwidth of a GHFS. The first resonance peak gives approximately about 20 dB of gain at the resonance frequency circa 20 MHz and at the top of the bandwidth of the sensor, which is 17.7 MHz, the gain is about 12 dB. This is way off ± 3dB of the base amplitude when considering the bandwidth of the instrumentation. It can be deduced that badly designed wiring can cause measurement error when working on the area, where the system resonates. The measurement errors can be seen as overshooting, slow settling time at step responses or wrong amplitude in transient measurement.

Transverse Seebeck effect is a self-generating voltage source which means that no drive circuits or measuring bridges are needed. Sensors based on transverse Seebeck effects are also able to produce linear output of the measured value. Thus, instrumentation should perform only linear actions to the signal and have a voltage amplifier. Due the low levels of the output signals generated by sensors, signal conditioning needs an amplifier, which should have high input impedance but small input capacitance to prevent voltage division at the input of the amplifier.

The equivalent circuits in figures 3.6 and 3.5 were created from measurements with a GHFS but they are also applicable to other transverse Seebeck heat flux sensors. Although, they might have different structure, like a single rectangle block instead of multiple elements, because it is always in series with the wiring and creates loop with it. Transverse Seebeck effect sensors have the internal resistance, which is determined by the material of the thermo-element, but also they have series inductance and parallel capacitance. The inductance varies with the area of the loop and the platform material, because it affects the surrounding permeability. Wiring should be taken care when designing a HFS based on transverse Seebeck effect, since its capability to high frequencies are verified in several studies [21][22][23] and the wirings creates the parasitic components that are large enough to affect frequency response and seen in the higher frequencies. When amplifier is placed near as possible to the sensor, one can use simplified model of the system without the cable parameters, because wiring is included to the sensor.

4 THE CASE

In this chapter the problems of the case is solved. First is studied the electromagnetic interference caused by the electrical motor. After that the signal chain of instrumentation is specified. Then a design of an amplifier for the case is shown. The amplifier is simulated and built. The performance of the designed amplifier is tested. At the end of the chapter there is a review about the results of this thesis.

When accurate measurement is wanted, there is needed to be sure that measurement contains only the signal. One factor that affects the instrument outside its circuit is environment or ambient. In this Thesis the environmental load is examined only for the case of the study, because the ambient is application specific. For the electronics, an electronic motor is noisy environment. Therefore, EMI coupling to sensors should be studied. In addition to EMI, there is also possibility of high temperature for the electronics. In this part, the same setup used by Jussila et al. [6] is tested. In addition to Jussila's setup, another sensor has been installed on a stator tooth. The location of both sensors is presented in figure 4.1.

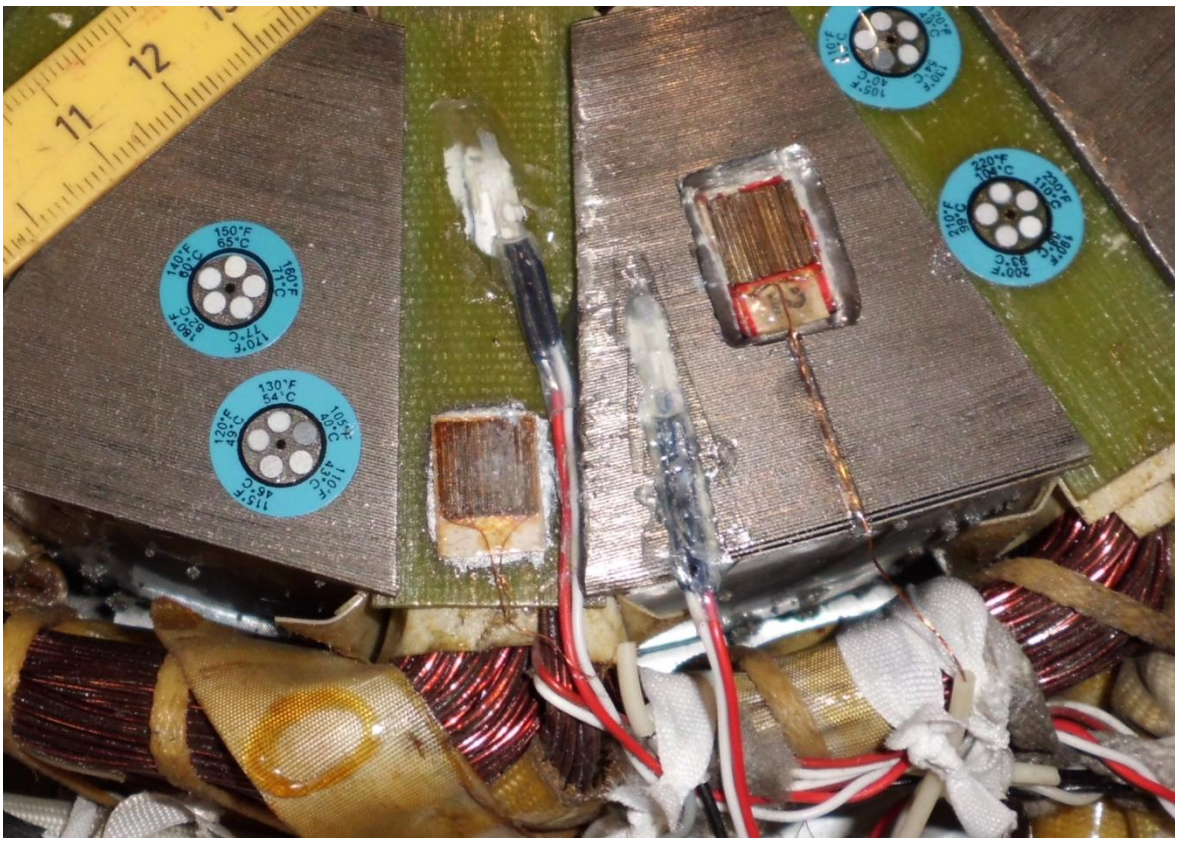

Figure 4.1 One stator stack of the motor, with two GHFSs installed on stator tooth and stator slot. Also various PT100-temperature sensors installed near heat flux sensors.

From figure 4.1 can be seen that both sensors are very close different noise sources. The sensors are placed in the air gap and near the windings of the motor. The windings are potential noise source because the windings are where the power is brought to the electric motor. While the electric motor is driving a load, current passes through the winding. As currents are going through winding, they not only produce magnetic flux, but noise sources in series with the sensor circuit via mutual inductance and are proportional to applied current.

4.1 Signal, noise and coupling

Signal is anything electrical quantity (voltage, current) which is known and wanted. Noise is everything else. Noise coupling can be categorized to two types: differential and common mode. Differential mode noise source in current loop can be place to series in the loop. Common mode noise is parallel to the closed current loop. Even the signal source can be the noise source. For example, it has too wide bandwidth related to application. [42] A right method for instrumentation is needed . It contains input filtering, amplifying, output filtering and data acquisitioning, respectively. Common property for whole signal chain is bandwidth, a device before one shouldn't block the bandwidth what next device needs. Therefore, the needed bandwidth should be specified and need to keep true when the signal reaches to the last device of the signal chain.

Any sensor, like a heat flux sensor or a thermometer, placed in the air gap of an electrical motor is affected by not only the magnetic flux of the air gap but close field coupling with stator windings. If the sensor's wiring is brought out form the motor through same way than winding cables of the motor then it is more likely cables of the sensor to be interfered by the all the power cables of the motor. Two main ways to couple EMI in close field is through mutual capacitance and inductance. There are also capacitive coupling between stator iron and the sensrors. If sensor is on a stator tooth like it is in the case, then capacitive coupled noise from stator tooth creates common mode voltage to sensor input. Capacitive coupling creates parallel voltage source with conductors, but more concerning thing is common mode voltage created by capacitance between stator tooth and the sensor against the motor ground. Electric motors are usually driven by frequency converters. The power output of a frequency converter can be filtered but the frequency of switching could be seen at input voltage of the motor. The switching frequency varies from several kHz even to 1 MHz. Via capacitive connection from wounding and stator iron to the sensor, switching noise and the fundamental drive phase voltage can create common mode voltage to the amplifiers input.

The motor is 3-phase power input, so it creates three of both capacitive and inductive EMI sources. Since the phases has different position on motor and therefore they have different parameters for coupling.

Since output voltage of a GHFS is under 1 mV in this application, thermal noise can be very problematic when temperature raises to motor's maximum operating temperature. Therefore, Johnson noise is a significant noise source, so it is taken into account to total noise. The sensors have internal resistances of 7.11 Ω and 10.97 Ω, which spectral noise densities are 0.34 nV/Hz$^{-1/2}$ and 0.42 nV/Hz$^{-1/2}$ respectively, according to (2.20). The input impedance of the amplifier is large it isn't related to Johnson's noise, but it input noise can be read from the amplifier datasheet. On the other hand, the input filter contains resistors, which add Johnson's noise. The load noise is added as noise source also.

A sensor in a motor's air gap gets distorted by many sources. In figure 4.2 equivalent circuit for signal loop of a sensor with the noise sources descripted above.

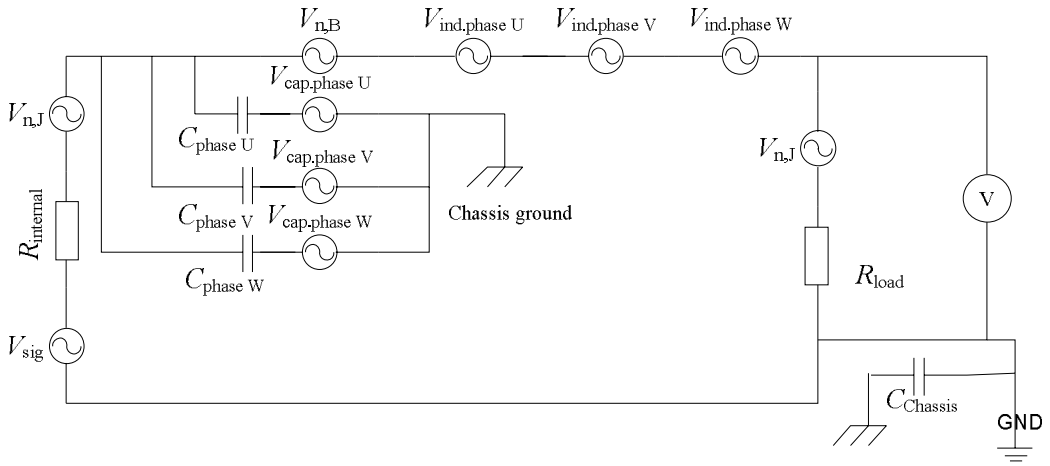

Figure 4.2 Noise model for a sensor in an air gap of an electric motor.

In figure 4.2 can be seen that there are many error sources and they should be minimized as low as possible. The noise voltage creates current to sensor loop. When this noise current is applied to a heat flux sensor, it creates transverse or longitudinal Peltier effects to the sensor. As equation (2.7) shows that the transverse Peltier effect is proportional to current density. Current creates heat flux through the sensor and may override Seebeck voltage. In case of GHFS, the sensor is made of multiple small ATs instead of one bigger component, which means that the smaller width and height of the AT, the more affected GHFS is to transverse Peltier effect created by noise current.

The worst interference which could affect the sensor signal is caused by magnetic flux in the air gap. The magnitude of magnetic flux noise $V_{n,B}$ is studied. To investigate coupling of the magnetic flux in the air gap, the motor was ran by external electric motor. This way signal is only interfered by magnetic flux created by permanent magnets on the rotor. If the rotor is rotated by powering the stator, the signal is interfered by stator winding via capacitive coupling and mutual inductance. Also stator is not intentionally heated, but inevitably eddy currents, created by rotating PMs, the stator will get heated, but will left unnoticed.

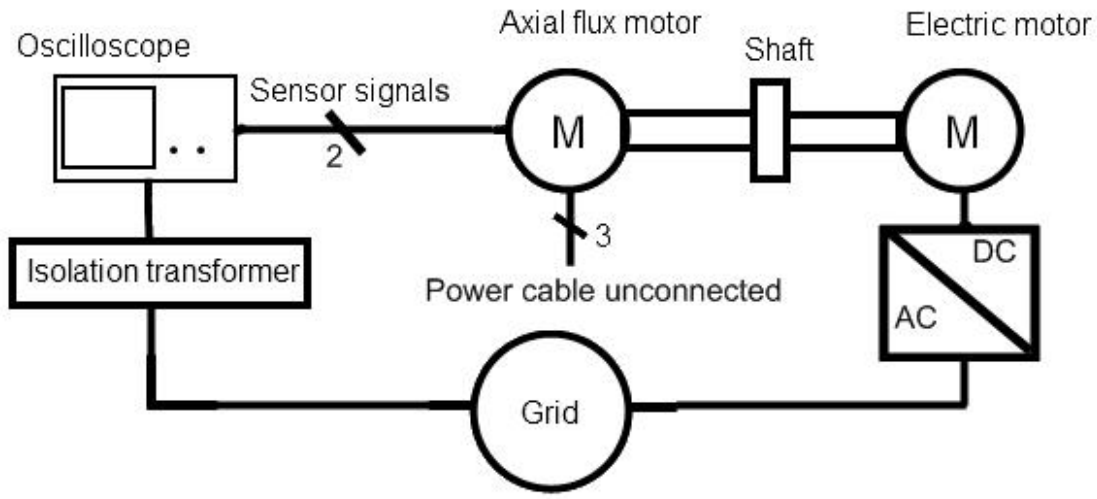

Figure 4.3 Test setup for the sensor output when rotating only the rotor of the motor with external electric motor.

Speed of the rotor was slowly increased up to 801 rpm. Both sensors were measured simultaneously with Tektronix TDS3052 oscilloscope. Figures 4.4 and 4.5 are measured voltage of sensors' signal output.

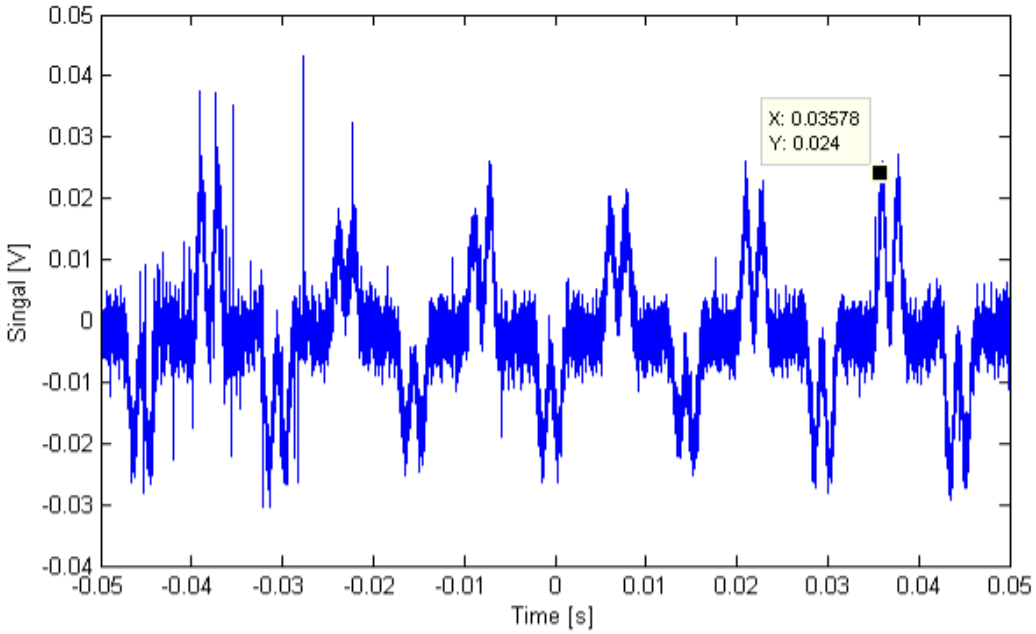

Figure 4.4 Output of the GHFS on the stator slot, when the rotor is externally rotated at 801 rpm. The sensor didn't have active heat source.

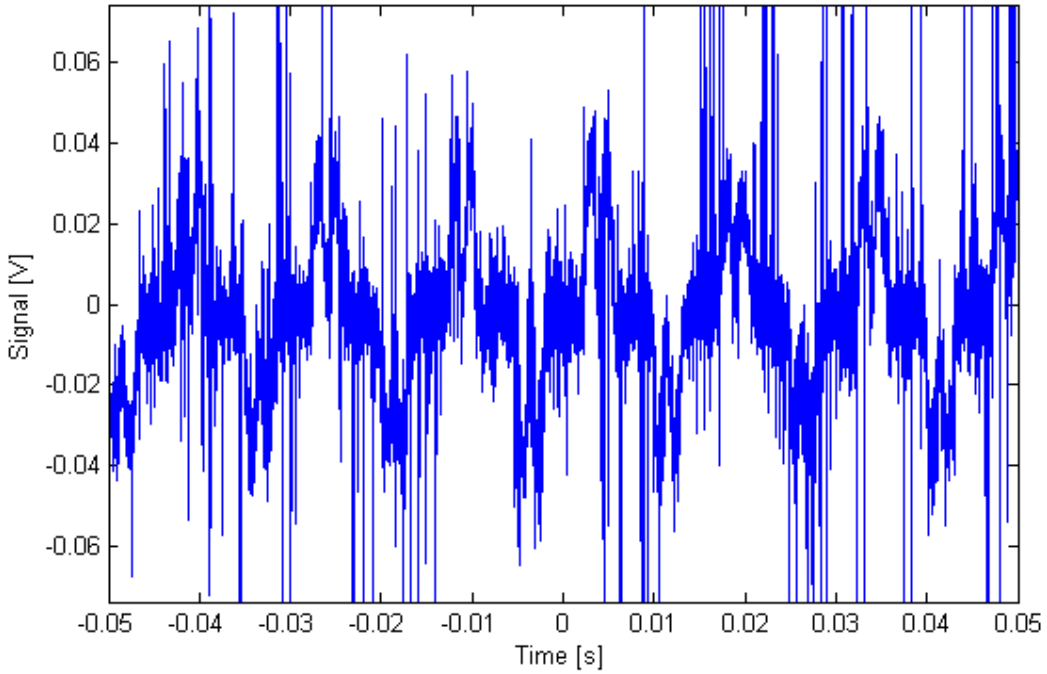

Figure 4.5 Output of the GHFS on stator iron when the rotor is externally rotated at 801 rpm. The sensor didn't have active heat source.

From figures 4.4 and 4.5 can be seen a lot of noise and the signals are not observable. In figures 4.4 and 4.5 can be seen that a periodic waveform appears. This can't be the signal

of the sensors created by transverse Seebeck effect, because it is changing polarity at rate faster than Jussila et al measured [6] and no significant heat source is present. Both signals have similar output waveform. Also it was noticed that amplitude and period of the signal was proposal of rotating speed from which can be deduce that sensors are affected by magnetic flux. FFT analyses are made for the measured data to prove the assumption that the measurement contains mostly induced voltage. FFT or Fast Fourier Transform tells the frequency content of analyzed data. FFT analyses are presented in figures 4.6 and 4.7. The calculation was made with MATLAB and the FFT-algorithm is in Appendix III.

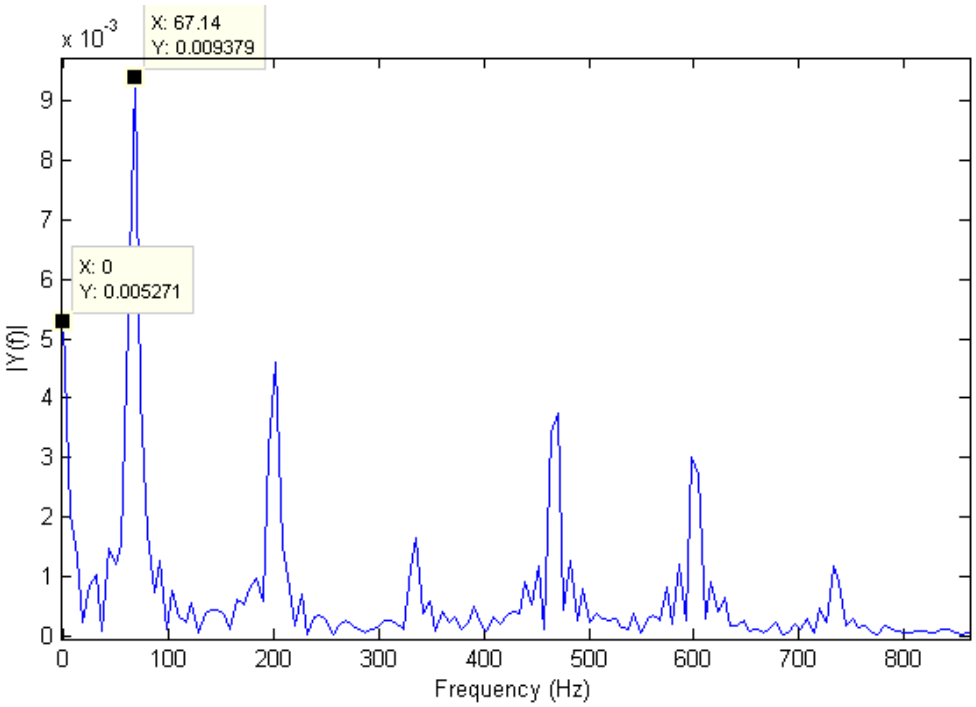

Figure 4.6 FFT analysis of the output signal of the GHFS on stator slot from figure 4.4

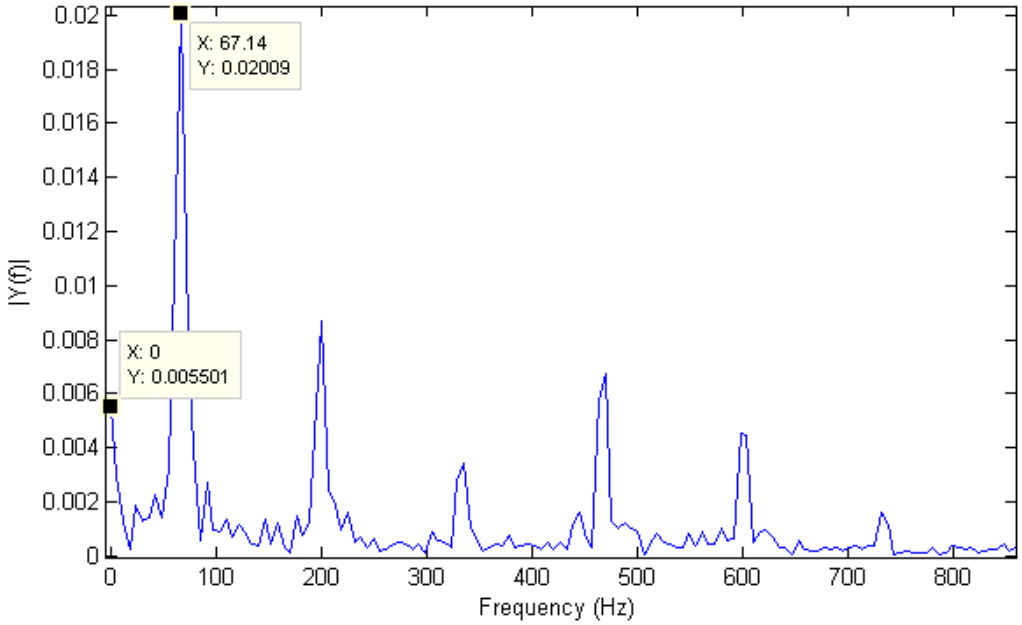

Figure 4.7 FFT analysis of the output signal of the GHFS on a stator iron.

The period of the periodic waveform is about 0.015 s, which corresponds to 67 Hz. From signals presented figure 4.4 and 4.5, FFT analysis was made and results is presented in figure 4.6 and 4.7 respectively. From the FFT analysis we can see frequency of 67 Hz as the highest peak. Although the inducing frequency of flux is double of that, because it reaches constant flux density before it changes polarity. Therefore, flux density changes two times, before the direction of magnetic flux changes, which yields 134 Hz for the frequency of the magnetic flux. The waveform of the induced voltage is not pure sine wave, the slotting effect causes the flux aligns straight to high permeability material, in this case, towards rotor teeth. [25] This slotting effect causes flux density to change proportional to the position of the magnets, which creates harmonics to the induced voltages. Figure 4.8 shows flux density of the air gap at different positions of permanent magnets.

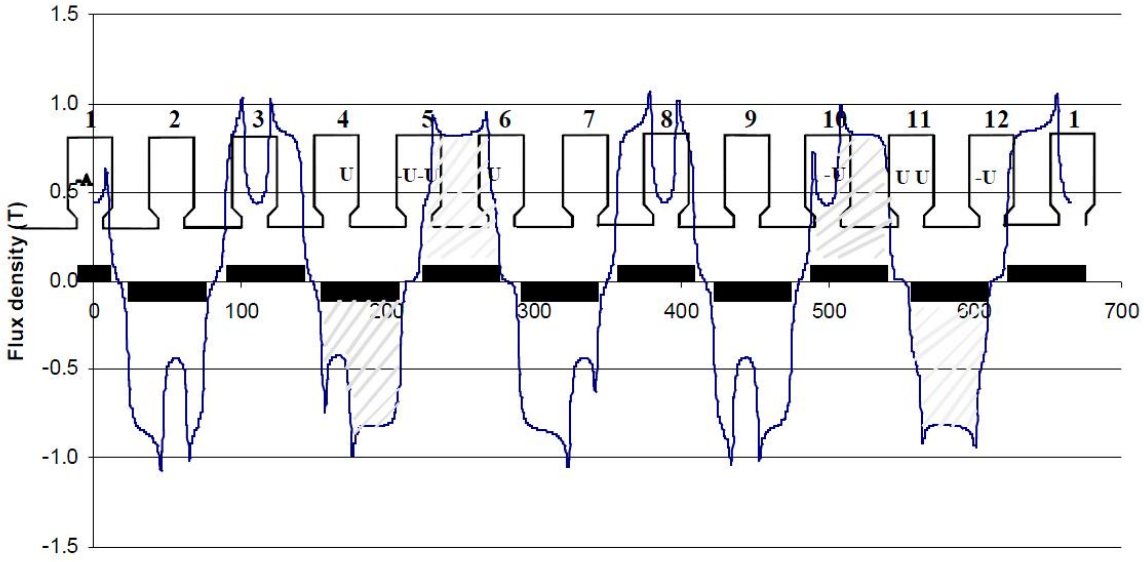

Figure 4.8 Air gap flux density and positions of permanent magnet of an axial flux machine at a certain radius. [8] From figure can be seen that flux changes two times when it passes a rotor tooth.

From figure 4.8 can be deduce that flux density changes two times when a single magnet passes the sensors. Due the slotting effect seen in figure 4.8, the noise wave form is not sinusoidal. The sensor and the signal wires create a loop which magnetic flux passes through. From figure 4.9 can be seen the sensor at the stator slot and the loop created by the sensor and the signal wires. This creates loop area which affects the induced voltage.

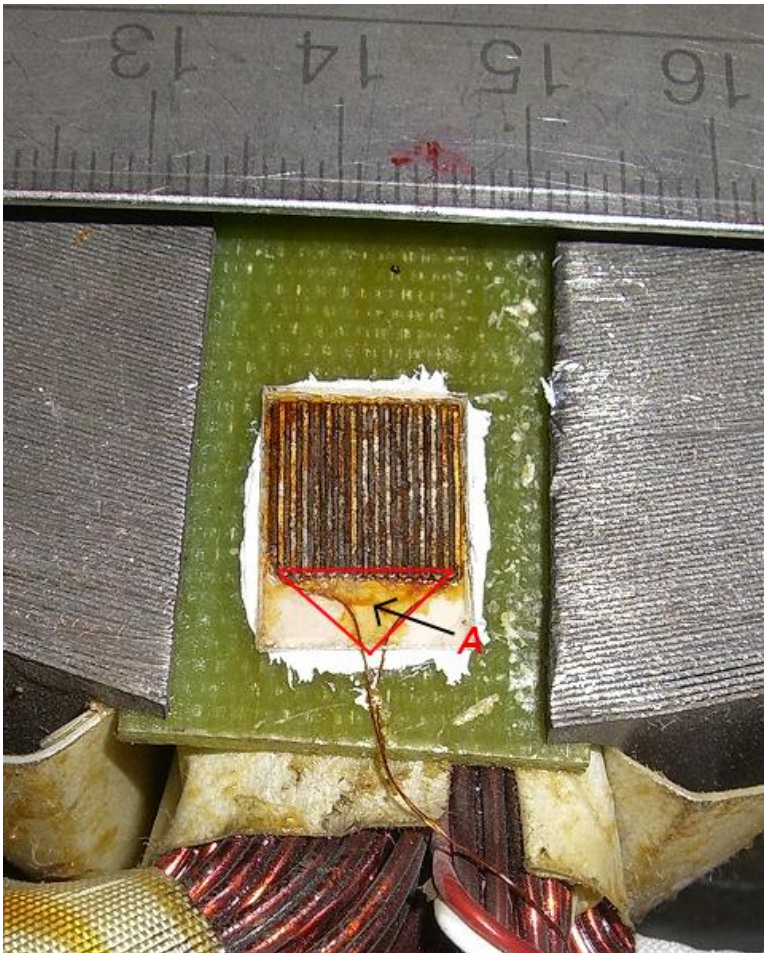

Figure 4.9 The sensor on a stator's slot. Wires and the sensor create a loop which area *A* can be approximated. Modified from [6].

The magnetic flux is affected to the loop formed by sensor and wiring. The approximated loop area of the sensor and signal wires on the stator slot is 0.00003 m^2. The maximum flux density of permanent magnet is 1.1 T and frequency *f* is rotating frequency of the rotor multiplied by rotor poles, 134 Hz. Substitution to equation (2.8) gives absolute value for a peak voltage 27.7 mV when cos θ = 1, which correspond well to measured peak values 24.0 ... 28.1 mV in figure 4.4. At faster rotating speeds the peak voltage of induced noise enlarges. At the nominal speed, the calculated peak voltage would be 75.4 mV.

The periodic signal of figures 4.4 and 4.5 is generated by magnetic flux and the non-sinusoidal waveform is caused by slotting effect. Because of the polarity change of permanent magnets the signal is seen as frequency of rotating frequency of the rotor multiplied with pole pairs. There by 5*801 rpm / 60 rpm*Hz^{-1} = 67 Hz.

The amplitude of the induced voltage is greater than the signal measured by Jussila et al [6], where their measurement gave values around 170 µV at 2400 rpm. As the noise is created at the same frequency as PM passes, measuring the fluid speed or thermal radiation

absorption of PMs becomes impossible. The noise voltage creates current through the sensor, which creates transverse Peltier effect. Also it is possible that copper wiring and the sensor create thermocouple and longitudinal Seebeck effect is seen when fluid flows in the air gap.

4.2 Methods to minimize error sources

Frequencies outside of the required bandwidth are noise. It is required that filters are implemented before and after the amplifier. At first should protect the signal from noise. By shielding signal wires, protects from both close field coupling, capacitive and inductive coupling. The shield needs to be grounded, in order to work. If shield doesn't cover whole length of the wires, the shield loses its effectiveness. [26] [27]

For reducing the common mode and other noise, the amplifier input is chosen to be differential. Therefore, the both wires need to be unconnected to ground. The shield is then grounded only and it needs to be done properly. According to experimental data made by Ott [ott], a suitable shielding method for this case is to shield both wires and ground the shield only at the amplifier end of the cable. This method, which is presented in figure (x.x), provides 70 dB attenuation. Attenuation values were referred to case where the loop was grounded at both end and shield was left ungrounded. For a comparison, twisted pair cabling with six turns/ft had attenuation of 55 dB. [27]

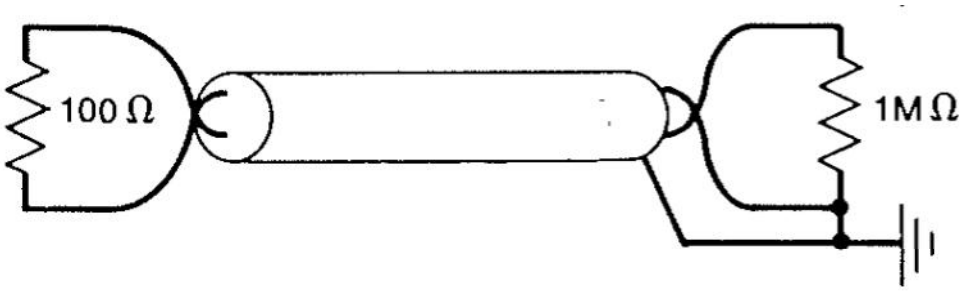

Figure 4.10 Proposed cabling method to improve protection against noise caused by inductive coupling. [27]

It can be deduce that EMC of the measuring setup is noticeable improved by using shielded cable for heat flux sensors instead of twisted pair cabling.

For measuring heat flux inside of the electrical motors, should the wiring be optimized and shielded. If it is possible, the wires should go along the magnetic flux. Since the frequency of magnetic flux is proportional to rotating speed, it is not possible filtered out from the signal. There are various methods to calculate out the flux noise, but those are not included in this thesis.

If the sensor is protected from magnetic flux by a metal foil or such, the signal is delayed by the thermal resistance and thermal capacitance of the protective material and the insulation layer. The protection is then a mechanical low pass filter for the sensor. In addition the metal shielding could get heated by eddy currents caused by magnetic flux.

While some of the noise sources are proportional to the ground of the electric motor, the interference is damped when the measurement electronics is disconnected from the ground of the motor. Isolation is a solution to break the ground connection. Also differential input amplifiers block the ground loop for the common mode noise sources. [27] These are mainly common mode noise sources which travel in both signal wires. Common mode noise sources create noise voltage to load when current coupled through mutual capacitance to the sensor's load. Differential input amplifiers amplifies voltage difference between its inputs, so theoretically common mode noise is blocked while it appears symmetrically on both signal wires. Adding an amplifier near to the sensor creates a buffer between sensor and common mode noise sources.

The EMC should be corrected, before using amplifiers in the system. The noise made by magnetic flux could saturate the output of an amplifier, depending on input ranges and gains of the amplifiers. The amplifiers should be placed as close as possible to the sensor to enlarge the signal level to improve signal to noise ratio. The amplifier will be affected by magnetic flux and inductive and capacitive coupling with motors windings. Therefore, it is important to shield entirely amplification circuit with an enclosure. Another way to protect from EMI inside the motor is create the circuit small as possible. Another reason for small implementation of the circuit is limited space inside the motor.

4.3 Requirements for components

The measuring environment sets the requirements for component selection. As noted, temperature difference is present when measuring heat flux. Sometimes the amplifier unit can be placed thermally apart from the sensor. In many cases that is impossible and amplifier unit is affected by a heat source. While temperature can be great it is important to choose components which can tolerate such temperatures. The maximum temperature of a GHFS is 271 ^{0}C. Without cooling system amplifiers cannot be applied up to that temperature. The maximum junction temperature for silicon components could be 125 ^{0}C, but there are components with maximum operating temperatures as high as 210 ^{0}C. The passive components have also temperature limitations

In our case, the stator surface of the machine reaches over 90 ^{0}C and can be higher, when the electric motor is loaded. The demagnetization temperature of the neodymium permanent magnets is 100…150 ^{0}C. [7] [8] For the case is suggested to place the amplifier circuit near the sensors. The sooner the signal is amplified and filtered, the better signal to noise ratio. Unfortunately the sensors are on the stator which is a heat source. Temperature can vary from room temperature 20 ^{0}C to maximum operating point of the motor even 100 ^{0}C. Temperature change is 80 ^{0}C and it is large enough to drift in amplifiers.

When possible magnetic field is present and it is fluctuating, first to do is keep loops small and shield the circuits. Using smaller components is easy way to minimize loops. Sometimes, smaller and more accurate components cost more so matching of components is required. For example, there is no advantage use smaller passive component with ICs which has wider lead gap than the passive component. Suggestion is to use size matched components, because even when using resistors larger than IC's leads, it is hard to minimize the loops.

Printed circuit board (PCB) is usually made from fiberglass with copper traces. Components which are soldered to copper traces can be made from different materials. Solder can be tin based alloy with lead or nowadays silver. Circuit implementation is then a mixture of various materials and it is easy to create thermoelectric effects on the PCB. On stable conditions, Seebeck effect won't be problem, but near heat source may spoil the accuracy of the circuit.

Ground plane could create stray capacitance with signal traces. This additional capacitance will create an extra pole which affect to frequency response by lowering the phase margin or create unstable input for amplifier. Although ground plane will create noise barrier and heat dispenser for some components.

4.4 Amplifier design and results

When designing an amplifier it is always making compromises. Since there are no ideal components, which are made to achieve some performance in cost of other properties. This represents the fact that right component decision is priority for working design. In this chapter a signal chain for the case setup is introduced and discussed but designing part considers only the amplifiers

For proper signal conditioning, signal chain should be specified. The signal chain helps to understand how the signal is processed. For the first thing to find out is the needed bandwidth. Sensors are usually able to produce signal at larger bandwidth than necessary, so the

input filter should prevent too high frequencies, but must be keep in mind that the -3 dB limits for specified bandwidth meets in end of the signal chain. Signal chain consists of at least one filter and one amplifier connected to the DAQ. On the other hand amplifier needs a filter to prevent rectifying effect of RFI and filter unwanted frequencies then it can be used also as a signal filter. Therefore signal chain, which presented in figure 4.11, has two low pass filters.

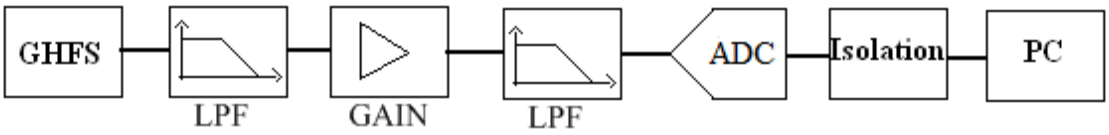

Figure 4.11 Proposed signal chain for the case setup.

Later low pass filter (LPF) in the signal chain of figure 4.11 can be implemented by active filter which also works as an output buffer. If amplifier is implemented with operational amplifiers filtering can be also implemented to feedback circuit, where amplifier itself acts like active filter with gain.

Isolation provides protection from ground loops. These ground loops can conduct EMI both from motor side but also from the data acquisition device. If a laptop PC, powered by battery, other grid isolation is not needed. For better signal fidelity it is recommended to not use analog isolators, but analog-to-digital converters (ADC) with an isolator because digital signals are able lossless signal transfer. Analog isolators have relatively small bandwidth. Signal of the ADC can be transferred with fiber optic or coaxial cable. On the other hand digital circuits near analog frontend could emit noise to analog part. If the amplifier's output is carried out by analog signal to DAQ. Cable length issues should also be taken care when using coaxial cable in digital transfer. The cable length should be considered, if the cable is not short according to wave length then a proper cable termination has to be done.

Power supply should be implemented with batteries and linear regulators. This way the amplifier is isolated from the electric grid. With low drop out (LDO) linear regulators one can reduce amount of batteries. One could use switched mode power supplies, but chopping creates more EMI. The noise from the power supply can be filtered with ferrite beads around the power cables and capacitors.

Certain parameters should be looked at when choosing the amplifier circuit. Whether to use operational amplifier or single IC implementation of the instrumentation amplifier,

there is some mutual parameters to look at. To decrease common mode noise, the CMRR parameter tells how well the amplifier depresses the common mode noise. Operational amplifiers have also internal power supply noise rejection, which ability to perform that is presented as power supply rejection ratio (PSRR). Power supply conducts also EMI, so the higher value of PSRR the better. The sensor itself has low output voltage level, thus a large gain is needed. The gain bandwidth product (GBP) tells about the amplifying capability of with proportional to bandwidth. This is used when speed is compared between operational amplifiers. Noise specification should be also inspected when a precision is preferred.

Instrumentation amplifier circuit made with operational amplifiers will be called a discrete instrumentation amplifier now on, and it means that the amplifier is not made from discrete transistor but separate operational amplifiers. A discrete instrumentation amplifier has a benefit to modify the design to obtain higher gain and larger bandwidth than commercial amplifier has to offer, because the circuit inside the integrated circuit (IC) cannot be modified externally. Although a discrete implementation has few set back that affects on its signal fidelity. Using a single package IC instrumentation amplifier, gives some advantage compared to the separate operational amplifier implementation. A discrete instrumentation amplifier has more external components, thus larger circuit area. The PCB will cause additional parasitic capacitance and inductance, what affect frequency response of the amplifier. Despite the frequency response, the phase response is also under inspection when considering the signal fidelity.

As other thermoelectric studies which were reviewed earlier suggest and to decrease common mode noise, a differential type amplifier topology is chosen. High input impedance is needed to avoid voltage division with the internal impedances of the sensors. Also this prevents relatively large noise current to pass through the sensor, which could create measurement errors caused by transverse Peltier effect. Both requirements meet in an instrumentation amplifier, which is selected to be the topology of the amplifier design.

To find a correct amplifier component for instrumentation, should the data sheets and specification studied and look for the desired values that the case needs. In our case, a low offset with good DC performance is required. In tables 4.1 and 4.2 is listed operational amplifiers and in table 4.3 instrumentation amplifiers with generally good values to heat flux measuring. The amplifiers to the tables are gathered from different manufacturers, with the most suitable values for the case. The inspected variables for operational amplifiers are input offset and its drift, *GBW*, G_{ol}, noise specification, input capacitance C_{in} and *CMRR*.

Table 4.1 Comparison table for operational amplifiers I [43][44][45][46][47]

	Operational amplifier				
Variable	LMP2022	AD8629	OPA211-HT	ADA4895	ADA4528
V_{osi} [µV]	10	5	30	53	0.3
$V_{o,drift}$[µV/°C]	0.004	0.002	0.35	0.15	0.002
GBW [MHz]	5	2.5	80	236	3.4
G_{ol} [dB]	160	145	130	100	140
$e_{density}$[nV/√Hz]	11	22	1.1	1	5.9
e_{pk-pk} [nV]	260	500	80	99	99
C_{in} [pF]	12	1.5	8	3	16.5
CMRR [dB]	141	140	120	92	137

Table 4.2 Comparison table for operational amplifiers II [48][49][50][51][52]

	Operational amplifier				
Variable	LT1050	MAX44252	TLC2652AM	ISL28134	HA-5147
V_{osi} [µV]	0.5	3	0.5	0.5	50
$V_{o,drift}$[µV/°C]	0.01	0.005	0.003	0.0005	0.4
GBW [MHz]	2.5	10	1.9	3.5	120
G_{ol} [dB]	160	154	150	174	123
$e_{density}$[nV/√Hz]	-	8	94	1	3.2
e_{pk-pk} [nV]	1600	5.9	800	10	90
C_{in} [pF]	-	2	-	5,2	-
CMRR [dB]	120	140	140	135	120

For the instrumentation amplifiers, variables under inspection are input offset V_{osi}, and its drift, bandwidth (BW), gain error and nonlinearity, gain drift, noise specifications, input bias current and *CMRR*.

Table 4.3 Comparison table for intrumentation amplifiers [53][54][55][56][57][58]

	Instrumentation amplifier					
Variable	AD8421BRM	AD8229	INA128	LTC110	ISL28617	MAX4208
V_{osi} [µV]	50	100	50	1	30	45
$V_{o,drift}$[µV/°C]	0.9	0.1	0.5	0.005	0.3	0.1
BW[kHz]*G*=100	2000	1200	200	18	2000	7.5
G_{error} [%]	0.2	0.3	0.5	0.01	0.004	0.35
$G_{nonlinearity}$ [ppm]	40	2	1	3	-	25
G_{drift} [ppm/˚C]	-50	-100	1…10	4	-	50
$e_{density}$[nV/√Hz]	3	1	8	-	8.6	140
e_{pk-pk} [nV]	0.07	0.1	0.2	1.9	-	2.5
I_{bias} [nA]	0.1	70	2	0.065	0.2	0.01
CMRR [dB]	80	80	120	90	120	90

The tables are collected from the manufacturers' datasheets and values used are typical values. If the typical value was not provided, the value, which is worse, is in the table instead. Line in the table, means that datasheet didn't provide that value.

When considering the amplification of transverse Seebeck effect heat flux sensors in generally. There weren't many amplifiers, which are able to amplify full bandwidths of a GHFS or an YBCO film, with tolerable offset parameters and capable to high gain. Such fast single IC instrumentation amplifier is not available. Therefore, if needed one, a discrete instrumentation amplifier with operational amplifiers with capability to amplify that bandwidth at gain of its stage. Also it might be needed to divide the gain between the input and output stages. This lowers the gain needed from a single operational amplifier and improves CMRR of the output stage, according to the equation (2.17). For example ADA4895 has the bandwidth of 236 MHz, when the gain is 10. It should be noticed, that ADA4895 is stable when $G \geq 10$. Therefore, it is compulsory to divide the gain between input and output stages, when an instrumentation amplifier is made with ADA4895s.

Fortunately, the case requires a lower bandwidth than the maximum bandwidth of the GHFS. The measurements made by Jussila et al [6] shows that at DC frequency at nominal speed the output voltage of the sensor on stator slot rose to circa 250 µV and the smallest signal varied by 1 µV. It is wanted to see of heat flux measurements the effect of radiation power of a single magnet. The motor have the nominal speed of 2400 rpm and 10 magnets in the rotor. The signal bandwidth is set to be ten times the frequency of magnets at nominal speed, which yields 4 kHz.

The amplifier is wanted to have bandwidth which doesn't attenuate the signal. The bandwidth of the amplifier is chosen to be 20 kHz to prevent signal from attenuation and have the gain G = 1000.

Suitable single IC instrumentation amplifiers are AD8229 or INA128. They have good properties and available in high temperature packages, which allow to use the instrumentation amplifier at 175 to 210 ˚C of junction temperature. The real operating temperature is below that because available SOIC-8 packages have typical heat resistance of 100 W/K which is relatively large. On the other hand, operational and instrumentation amplifiers has low power dissipation, so the maximum junction and ambient temperatures are almost the same. An INA128 amplifier is available also as SOIC-8 with the maximum junction temperature of 125 ˚C. INA128 has good gain accuracy compared to others.

RFI-filter circuit should be after the sensor. Since the signal levels are low, one would like to prevent the voltage division on input filter and to prevent adding noise to the measurements, small as possible resistors should be used. RFI filter should be able to pass wanted differential bandwidth but it is impossible to have smaller bandwidth with common mode filtering than differential mode signal. By selecting 47 Ω using equations (2.13) and (2.14) can be the capacitors for RFI-filter circuit calculated, which yield values for capacitors C_1 = 100 pF and C_2 = 10 pF for the desired bandwidth which for RFI-filter is ten times higher than signal bandwidth.

For bias two grounded resistors are used. Their values are picked to be 200 kΩ and they should provide enough bias current and keep the sensor circuit impedance high to prevent noise current which generates transverse Peltier effect in the sensors.

Any amplifier in tables 4.1 and 4.2 could be used in the application but for the case is used LMP2022 because it has a high open loop gain and is one of the smallest input offset parameters. It has also tolerable noise parameters. In addition, LMP2022 has built in electrostatic discharge - and EMI protection. Those attributes provide needed protection to the circuit without adding more additional components which yields smaller circuit area. LMP2022 can tolerate 125 ˚C at junction. Drawbacks are quite low operating voltages, voltage difference between power supply pins shouldn't be more than 5 V. This limits the input voltage span. The C_{in} isn't the smallest but it is not so important variable in our case, since the needed bandwidth is low and filtered. Open loop frequency response is used to determine how much amplifiers can amplify at certain frequency. In figure 4.12 is presented Open loop frequency response of LMP2022 and the circuit parameters.

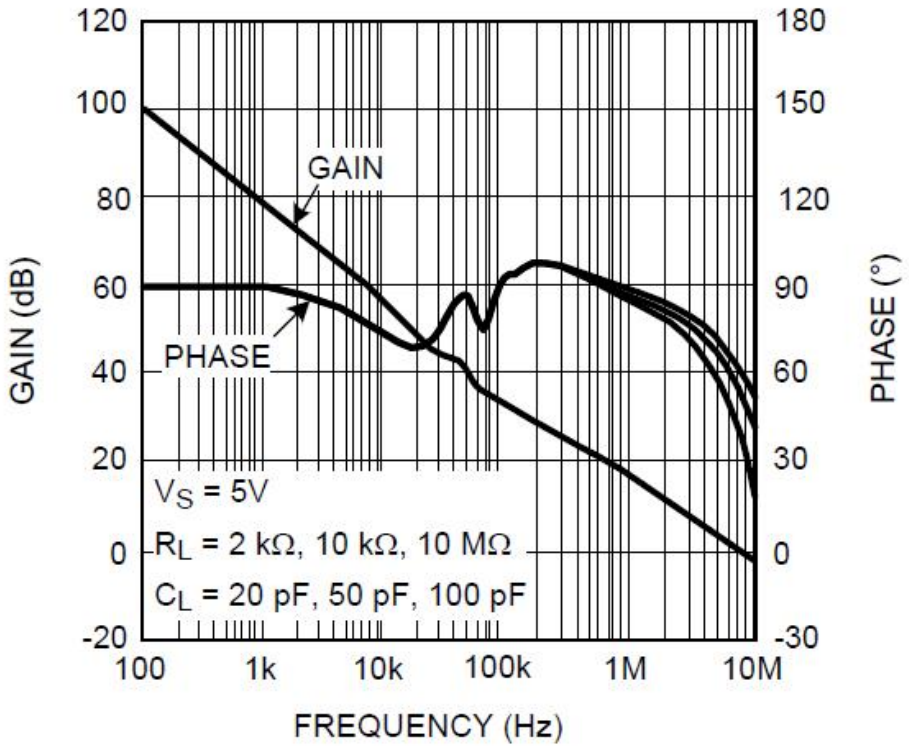

Figure 4.12 Open loop frequency response of a LMP2022 operational amplifier. [43] A designer should always check bandwidth of the needed gain of the operational amplifier from the open loop frequency response diagram.

When looking the gain curve in figure 4.12 and one can see that at 60 dB open loop gain, which is equivalent for 1000 in linear scale, doesn't reach desired 20 kHz. So it is needed to divide gain to the instrumentation amplifiers output stage when using LMP2022 operational amplifiers. It is important to give for the input stage more gain to get better CMRR and the output stage won't amplify too much errors caused by the input stage. The gain for the input stage is chosen 40 dB and for the output stage 20 dB which is together 60 dB. The bandwidth of the input stage, with gain of 40 dB, is 50 kHz according to figure 4.12. For the output stage it, the bandwidth is circa 650 kHz when the gain is 20 dB. With these gain settings an discrete instrumentation amplifier with LMP2022 amplifiers will reach minimum 20 kHz bandwidth with gain of 60 dB.

Choosing feedback resistors for the amplifier should be chosen wisely. Large resistors are noisy but small resistor may over load the amplifier. The maximum output current and the maximum output voltage determine the minimum load with Ohm's law, which is, in a case of a discrete instrumentation amplifier, are positive feedback resistors of the output stage. One should also read from the datasheet what load is needed to reach the performance an-

nounced in the datasheet. The datasheet of the LMP2022 suggest that the load should be at least 2 kΩ.

The gain of an instrumentation amplifier can be calculated by the equation (inst.amp), but for the gain of a single operational amplifier in the input stage of the discrete instrumentation amplifier can be calculated with the gain equation of the non-inverting amplifier (2.15) and the output stage with the gain equation of the differential amplifier (2.16). The input stage was wanted have gain of 100 and the gain of the output stage then will be 10. There are available only fixed size resistor, so the gain of the input stage is set to 101 for making the selection of resistor easier. Now the total gain is 1010 or 60.09 dB, which yields with the gain equation of an instrumentation amplifier (2.18) values for the resistors: R_f = 2 kΩ, R_{in} = 200 Ω, R_{FG} = 1 kΩ, R_G = 20 Ω.

The DC gain accuracy can be calculated with equation (2.22) which yields for operational amplifiers of the input stages $22*10^{-6}$ % of accuracy at typical G_{ol} = 160 dB and 0.0039 % at worst case when G_{ol} = 115 dB. The circuit was simulated with TINA TI v.9 simulation software. In figure 4.13 is presented the circuit of the designed amplifier in the simulation software. To the feedbacks of operational amplifiers, there were added filtering capacitors to filter higher frequencies.

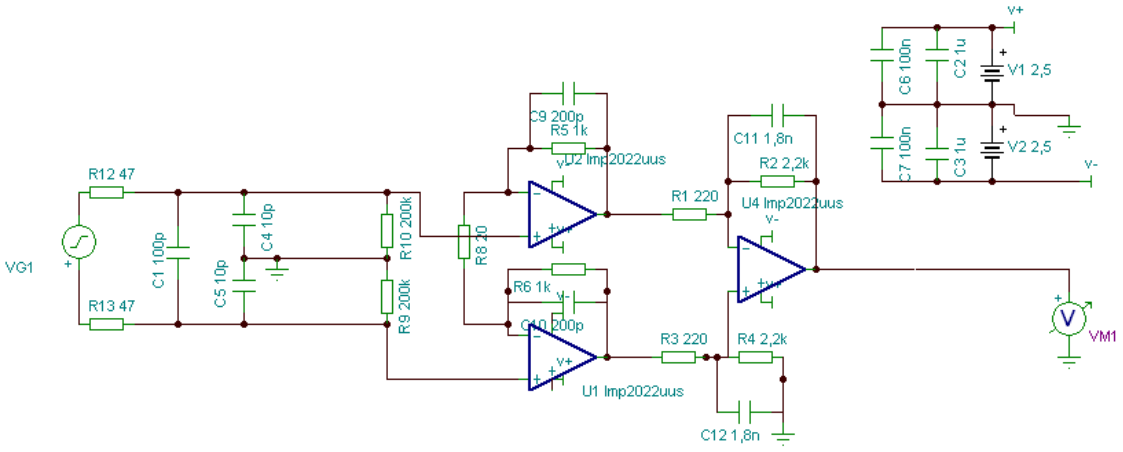

Figure 4.13 The designed amplifier circuit constructed in the simulation software.

In the simulator figure 4.13, there is as source, sine wave voltage generator VG1 and input device VM1. Now the amplifier is complete and the software is used to simulate amplifiers AC-response, which yields the Bode plot of the amplifier in figure 4.14.

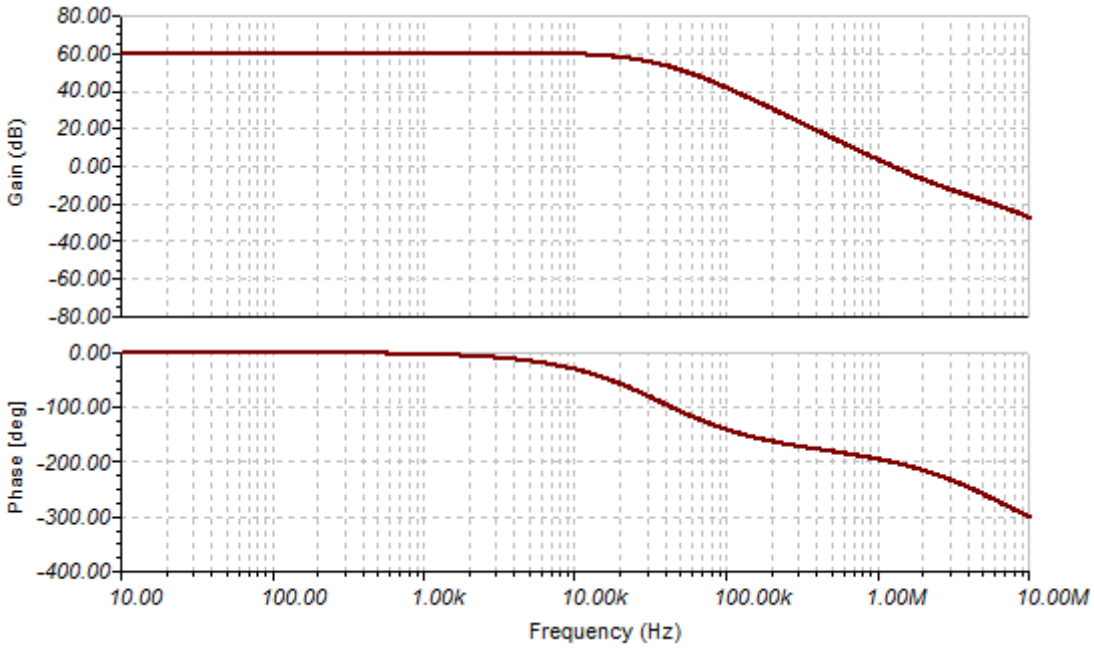

Figure 4.14 Simulated Bode plot of the designed amplifier.

From the simulated Bode plot can be seen that -3 dB point of the bandwidth of the amplifier reaches to 23 kHz, which is more than wanted but signal bandwidth doesn't get attenuated. The gain at 4 kHz differences from DC gain 0.1 dB. The stop band attenuates at -40 dB/decade so input filter and the amplifiers itself acts as a 2nd order filter to the system. Nevertheless, there is still recommended to add a filter between the amplifier and the ADC.

The designed amplifier was built on a PCB which had place for two discrete instrumentation amplifiers. Operational amplifiers are provided in IC components which contain two amplifiers in one IC, so total of three dual operational amplifier ICs is required for two instrumentation amplifiers. For the test platform LMP2022s are in MSOP 8 packages and passive components are 0603 packages. They aren't size matched but used in the test platform anyway. Resistors had 0.5 % accuracy and capacitors were NP0/X7R classifications. CMRR for the resistor circuit of the differential amplifier can be calculated with (2.15) which yield 55 dB. The amplifier has ± 2.5 V supply voltage and BNC connectors for input and output. In figure 4.15 is the designed amplifier with only one channel build. There are placements for optional passive RC-filters for the outputs of amplifiers. The circuits and PCB layout is presented in Appendix IV. For the designed amplifier, the output RC filter was omitted and 0 Ω resistor was used to in the place of the resistor of the output RC-filter.

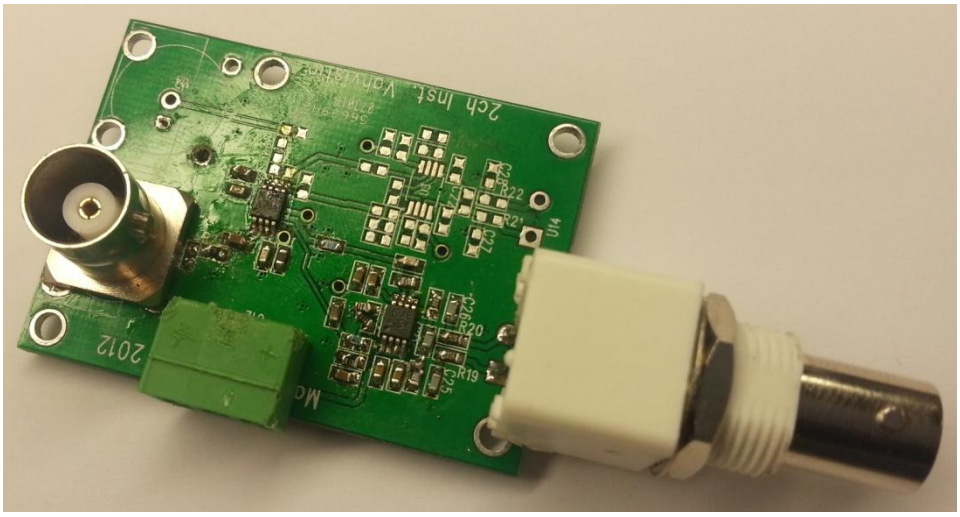

Figure 4.15 The designed amplifier built on a PCB. In the left, there is BNC connector for the output signal. The BNC connector for input signal is at the right. There is placement for an additional amplifier.

The designed amplifier has rail-to-rail capability in output and input. Thus, the maximum input voltage range is ± 2.5 mV. When the designed amplifier used for a GHFS with sensitivity S_0 = 10 mV/W and area A = 1 cm^2, one can calculated the maximum measuring range of heat flux with equation (3.1) which yields ± 2.5 kW/m^2.

The amplifier was tested with a Fluke 187 multimeter, Agilent 56420D oscilloscope and Hewlett-Packard 35670 Signal analyzer which has bandwidth of 51 kHz. First the amplifier was tested with the oscilloscope to confirm its functionality. The amplifier was connected to a signal generator which generated 1 kHz sine wave. The signal had peak to peak voltage level of 3.3 mV. Figure 4.16 shows the output signal of the amplifier from the screen of the oscilloscope and it can be seen that the amplifier is functional.

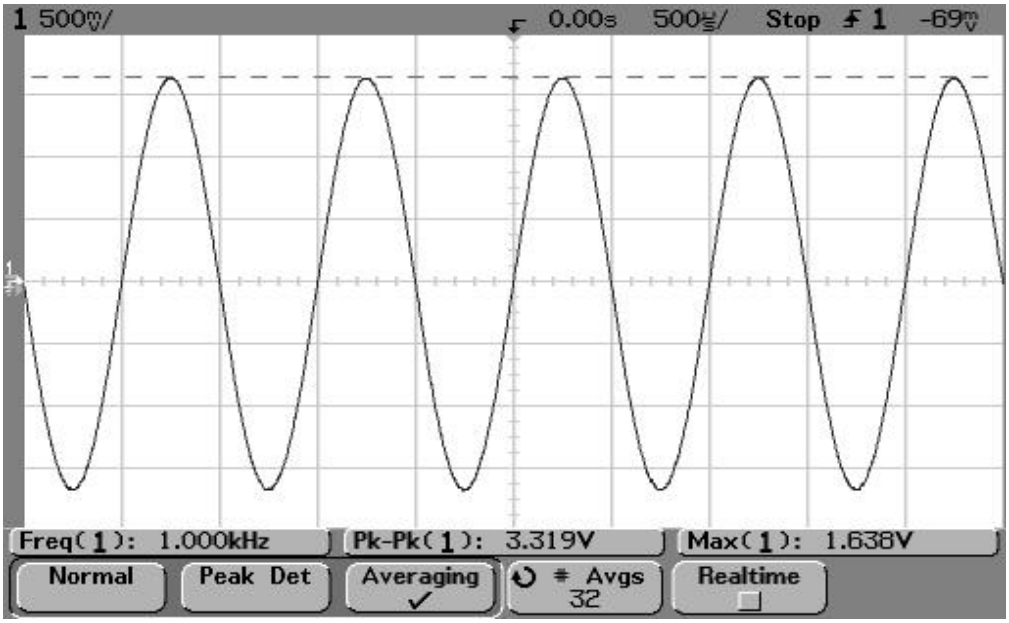

Figure 4.16 The output signal of the amplifier when the amplifier was supplied with 1 kHz sine wave from a signal generator. Voltage level of the input signal was 3.3 mV, which produced output voltage of 3.3 mV as seen in figure. The measurement was averaged with 32 times to suppress random noise of the input signal.

From the oscilloscope as in figure 4.16 can be verified that the amplifier is functional and is able to produce amplified output signal from input signal at desired gain of 1000. The output peak to peak level was 3.3 V which is same that input signal amplified with 1000.

The input offset voltage was measured with Fluke 187 multimeter. The input of the amplifier was short circuited and the output was measured with the DC voltage setting of the multimeter. The output voltage was 2.2 mV which is approximately 2.2 µV at input which is same as input offset voltage. When the input offset result is compared with IC instrumentation amplifiers in table 4.3, one can say that the designed discrete instrument amplifier performs well against IC instrumentation amplifiers in the table 4.3. The offset drift could not been tested as verifiable testing method wasn't available. But according to the offset drift parameter of LMP2022, the designed instrumentation amplifier should perform well in drift tests. In a simple test, the drift performance of the designed amplifier was estimated to be good enough. A verifying drifting test might need to be done in future to compensate the error caused by input offset drift.

The gain response was measured with the signal analyzer and the measurement result is seen in figure 4.17. The input voltage level was 1 mV_{rms}.

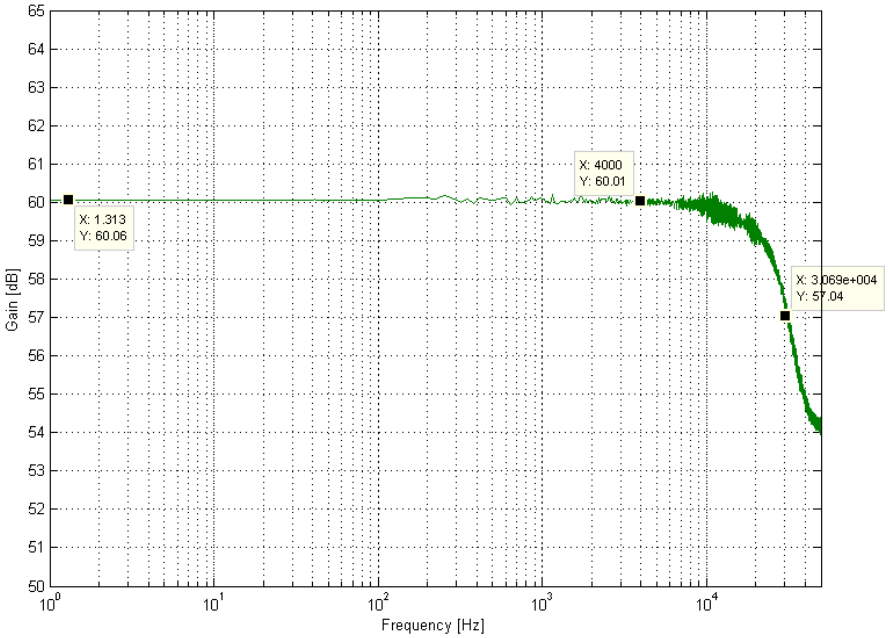

Figure 4.17 Gain of the designed amplifier with LMP2022 operational amplifiers.

The gain reaches the designed value of circa 60 dB. As seen in figure 4.17 the amplifier performs well on the signal bandwidth which is from DC to 4 kHz. The amplifiers bandwidth continues up to 30 kHz which is more than the value in the simulation in figure 4.14. The difference is explained by ± 15 % tolerance of capacitors but there is also unexplained nonlinearity in frequency response, which was found during tests without filtering capacitors and may be caused by the parasitic inductance created by an error in the design of the PCB of the amplifier. The error appears in 8 kHz to 40 kHz and affect to the gain as highest error in gain is + 0.6 dB and lowest - 0.4 dB. For future work, it is recommended to redesign the PCB with 0402 sized resistors and capacitor to match the size of MSOP8 packaged operational amplifiers and correct the signal loops. For the case, the PCB size should be minimized and use smaller connectors than BNC for the output of the amplifier.

4.5 Main results

An equivalent circuit for GHFS was presented in this thesis. and it turned out that it is a generally adoptable by all transverse Seebeck effect based heat flux sensors. The equivalent circuit is presented in figure 3.5. A sensor itself forms the resistor of the circuit and it is defined by the material from which the sensor is made of. The inductance and the capacitance are caused by the wiring and the dimensions of the sensor. Measured capacitance in GHFS was about 1 pF. The inductance of the sensor circuit is affected by the loop size and surrounding materials. The platform of the sensor will affect the inductance, because it changes the permeability of the surrounding of the sensor. The wiring loop should be mi-

nimized, because it reduces the inductance but also make the sensor less sensitive to interference caused by magnetic flux.

The case for this Thesis was the axial heat flux machine. Previously [6], its local heat flux in the air gap was measured with one GHFS. In this thesis, it was found out that the signal of the sensor is interfered by magnetic flux and also possible close field coupling of stator windings. Since, there is several error source is present and despite the measuring method, the measurement may contain error and the results of the previous studies should revised. Since the error sources was mapped out and solutions for them was presented, the measuring local heat flux instrumentation could be improved with EMC corrections. Although, the EMC correction and filtering could suppress the noise, but if the noise current travels through the sensor via capacitances in the measuring setup, the noise current creates transverse Peltier effect in the sensor. Then this opposite phenomenon alters the signal. Transverse Peltier effect is proportional to current density, which means that thinner material is more affected to noise current. Using wider thermo-elements in the sensor or a single block HFS could decrement the possible error caused by transverse Peltier effect. But it is only a marginal error compared to the interfered noise voltage. The amplifier is one solution for improving EMC in the setup by providing differential load for the sensors and placing the amplifier near the sensor the signal strength is raised before other EMI couples to the sensor. Unfortunately the noise from magnetic flux cannot be filtered out with analog filter, because frequency of noise of magnetic flux is proportional to the rotating speed of the motor. But when minimizing sensor loops and shielding the cables, the noise voltage could be reduced. EMC corrections should be done to prevent saturating the output of the amplifier.

The case gave many requirements for the amplifier. The temperature stability and DC accuracy with non-attenuated 4 kHz signal bandwidth and the gain of 1000 all together requires from one amplifier a lot. Several amplifiers were compared to find a suitable solution for an instrumentation amplifier. A discrete instrumentation amplifier was designed with LMP2022 operational amplifiers to produce low offset with accurate DC response and gain of 1010 for -3 dB bandwidth of 20 kHz to produce non-attenuated input signal. The discrete amplifier can be also a second order filter to the instrumentation with feedback capacitors, which is in the most cases, is impossible to IC instrumentation amplifiers. The result was that, the performance of the amplifier reached the design parameters. The cut off frequency were higher than designed but an output filter which is recommended to use before ADC, would correct the problem. Also one could use more filtering in the amplifier. The designed amplifier was not tested in the axial flux motor during this thesis. It would first need the required corrections to the measurement setup.

5 CONCLUSION

In this Master's Thesis a new sensor type was studied considering its instrumentation. The transverse Seebeck effect is long known phenomenon but until during recent decades it is been under serious studies. Before that, the study of the thermoelectricity was concentrated on longitudinal thermoelectric effects and their application like thermocouples and thermopiles. Transverse Seebeck effect studies are concentrated to materials and transverse Seebeck effect based sensors are mostly heat flux sensor, but their instrumentation has not been studied. At first the thesis purpose was to design and implement the amplifier for a heat flux sensors, and build a measuring device. During making this thesis, as knowledge gathered, it came up that it was needed to think more about instrumentation issues concerning about EMC and connectivity to the sensor. In this Thesis is created a model which describes electrical specifications of a transverse Seebeck effect heat flux sensor. The Thesis has a study case which was used to solve what kind of things could affect to heat flux instrumentation by the ambient of the electronics. The case was an axial flux electric machine with two installed bismuth transverse Seebeck effect heat flux sensors. These sensors are called by gradient heat flux sensors and they were used in this study to determine a general model to transverse Seebeck effect heat flux sensors.

Transverse Seebeck effect is capable to several nanosecond responses, since it is proportional to temperature gradient instead of actual temperatures of the sensor. Therefore, the equivalent circuit for sensors and loading effect was studied. The models were derived from bibliographic research and measurements. By using Thevenin's equivalent circuit and impedance measurement the equivalent circuit of the GHFS, can be proposed to be a voltage source with a low pass resistor-inductance-capacitance circuit. It is suggested that all transverse Seebeck effect heat flux sensor do apply the same equivalent circuit like the GHFS. The parasitic inductor comes from the loop which is formed by the wiring and the sensor itself. The inductance of the sensor model is also affected by the dimensions of the wiring and the permeability of the platform of the sensor. The cabling brings another RLC-circuit to the system which makes the whole circuit with an amplifier a 4th order system. This means that it has two resonance frequencies which may affect the signal band.

The models of instrumentations created in this thesis as well the equivalent circuits are universal to all transverse Seebeck effect HFSs than just to a GHFS. Also the noise model of the air gap is universal for any sensor in an air gap of an electric machine. The model could help for example other measurements that can verify the performance modeling of an electric machine.

Previous studies propose to use differential input amplifiers in thermoelectric instrumentation. In this thesis an instrumentation amplifier was designed for the case study. It was noticed, that in our case and possible in other heat flux sensing instrumentation as well, the instrumentation electronic could be affected by varying temperatures which may reach upper end of the temperature limit of components. These are source of measuring errors caused by the nature of semiconductor amplifiers, which means that choosing the right amplifier circuit plays important role in the amplifier design. The temperature related parameters of the amplifiers should be look at care. These are gain and offset drift. The more temperature stable amplifier the better. Noise specification should be compared too, because thermoelectric device has output levels from few µV to several mV. Too noisy amplifier could suppress the thermoelectric signal. The response times of transverse Seebeck effect and microvolt levels requires from the amplifier high gain and bandwidth product of the amplifier. Since in the case didn't require full band width of a GHFS the more important parameter was open loop gain, which determines the DC gain accuracy of the amplifier.

A discrete instrumentation amplifier was designed for the case. The discrete implementation was used to achieve desired bandwidth and gain with temperature stable operational amplifiers. The designed amplifier was built on PCB and its performance was tested.

The goals of this thesis were reached and its results are expected to help studies of thermoelectricity and electric motors. In thermoelectricity, there is potential to solve unclear step response tests. Apparently, the overshoot in response tests is caused by parasitic inductance in sensors. Using the equivalent circuit of a transverse Seebeck effect this overshooting could be minimized. In researches of electric motors, the measuring setup and its electromagnetic compatibility studied in this thesis should help the heat flux measurement gather more reliable and dynamic results for thermal modelling of electrical motors.

REFERENCES

[1] Dyer S. A., *Signal Conditioning*, The Engineering Handbook, 2nd edition chapter 153, CRC Press 2004. eBook ISBN: 978-1-4200-3987-0

[2] Webster J. G., The Measurement, Instrumentation, and Sensors: Handbook, CRC Press LLC, 1999, ISBN 3-540-64830-5, availability in Google Books.

[3] Incropera F. P., DeWitt D. P., Bergman T. L., Lavine A. S., *Fundamentals of Heat and Mass Transfer*, 4th edition, USA 1996, John Wiley & Sons, ISBN 0-471-30460-3.

[4] Diller T. E., *Heat Flux*, The Measurement, Instrumentation and Sensors Handbook on CD-ROM, CRC Press 1999, eBook ISBN: 978-0-415-87617-9

[5] Raphael-Mabel S., *Design and Calibration of a Novel High Temperature Heat Flux Sensor*, Master's Thesis, Virginia Polytechnic Institute and State University, 2005

[6] Jussila H. K., Mityakov A. V., Spozhnikov S. Z., Mityakov V. Y., Pyrhönen J., *Local Heat Flux Measurement in a Permanen Magnet Motor at No Load*, IEEE Transactions on Industrial Electronics, Volume: PP, Issue: 99, 2012.

[7] Howey D. A., Childs P. R. N, Holmes A. S., *Air-Gap Convection in Rotating Electrical Machines*, IEEE Transaction on Industrial Electronics, vol. 59, no. 3, pp. 1367-1375, Mar 2012

[8] H. Jussila, *Concentrated Winding Multiphase Permanent Magnet Machine Design and Electromagnetic Properties - case Axial Flux Machine*, Ph.D. dissertation, Acta Universitatis Lappeenrantaensis 374, Lappeenranta University of Technology, Finland, 2009.

[9] Rilla M., *Kestomagneettitahtikoneen lämpömallinnus*, Master's Thesis, Lappeenranta University of Technology, 2006.

[10] Derryberry R. A., *Artificial Anisotropy for Transverse Thermoelectric Heat Flux Sensing*, Master's Thesis, Virginia Polytechnic Institute and State University, 2007

[11] Seebeck T. J., *Magnetische Polarisation der Metalle und Erzedurch Temperatur Differenz*, Abhand Deut. Akad. Wiss. Berlin, 1822, pp. 265–373.

[12] Mann B. S., *Transverse Thermoelectric Effects for Cooling and Heat Flux Sensing*, Master's Thesis, Virginia Polytechnic Institute and State University, 2006

[13] Rowe D. M., *General Principles and Basic Considerations*, Thermoelectrics Handbook Macro to Nano, Chapter I, CRC Press, 2006, eBook ISBN: 978-1-4200-3890-3.

[14] Rowe D. M., Pollock D. D., *Thermoelectric Phenomena*, CRC Handbook of Thermoelectrics, Chapters 1 & 2, CRC Press, 1995, eBook ISBN: 978-1-4200-4971-8.

[15] Wilson J. S., *Sensor Technology Handbook*, 2005, Elsevier Inc., ISBN: 0-7506-7729-5.

[16] Reitmaier C., Walther F., Lengfellner H., *Transverse thermoelectric devices*, Applied Physics A, 2010, 99: pages 717–722.

[17] Thomson W., Mathematical and Physical Papers, Vol. 1, Cambridge Univ. Press, 1882, available http://archive.org/stream/mathematicaland01kelvgoog#page/n276/mode/1up

[18] Goldsmid H. J., *Transverse Thermoelectric Effects and Their Application*, Materials, Preparation, and Characterization in Thermoelectrics, Chapter 1, CRC Press, 2012, eBook ISBN: 978-1-4398-7471-4.

[19] Zahner Th., Stoiber Ch., Zepezauer E., and Lengfellner H., Transverse Thermoelectricity In A Tilted Metallic Multilayer Structure, International Journal of Infrared and Millimeter Waves, Vol. 20, No. 6, 1999

[20] Kyarad M., *Thermoelektrische und Photovoltaische Effekte in Metall-Halbleiter Multilagenstrukturen*, Doctor's Thesis, University of Regensburg, 2007.

[21] Mityakov A. V., Spozhnikov S. Z., Mityakov V. Y., Snarskii A. A., Zhenirovsky M. I., Pyrhönen J., *Gradient heat flux sensor for high temperature environments*, Elsevier, Sensors and Actuators A: Physical 176, 2012.

[22] Zeuner S., Prettl W., Lengefellner H., *Fast thermoelectric response of normal state $YBa_2Cu_3O_{7-d}$ films*, Applied Physics Letter, volume 66, Number 14, 3 April 1995, p. 1833-1835.

[23] Huber W. M., Li S. T., Ritzer A., Bäuerle D., Lengfellner H., Prettl W., *Transverse Seebeck effect in $Bi_2Sr_2CaCu_2O_8$*, Applied Physics A 64, 487–489, 1997.

[24] Pyrhönen J., Jokinen T., Hrabovcova V., *Design of Rotating Electrical Machin es*, 2008 John Wiley & Sons, Ltd. ISBN: 978-0-470-69516-6

[25] Pyrhönen J., Nerg J., *Sähkömagnetismi*, 2004, ISBN: 951-764-625-9.

[26] Morrison R., *Grounding and Shielding: Circuits and Interference*, fifth edition, John Wiley & Sons. 2007, ISBN 978-0-470-09772-4.

[27] Ott H. W., *Noise Reduction Techniques in electronic Systems*, John Wiley & Sons, 1988, ISBN:0-471-85068-3.

[28] Mohan N., Undeland T. M., Robbins W. P., *Power Electronics*, 3rd edition, 2003, ISBN 0-471-42908-2.

[29] Kitchin C., Counts L., *A Designer's Guide to Instrumentation Amplifiers, 3rd edition*, Analog Devices, 2006, available http://www.analog.com/static/imported-files/design_handbooks/5812756674312778737Complete_In_Amp.pdf.

[30] Floyd T., *Electronic Devices*, 5th edition. New Jersey, 2005, Prentice-Hall, Inc., ISBN: 0-113-973769-3.

[31] Millman J., Grabel A., *Microelectronics*, 2nd edition, McGraw-Hill, New York, 1987, ISBN: 0-07-100596-X.

[32] Spinelli E. M., Pallàs-Areny R., Mayosky M. A., *AC-Coupled Front-End for Biopotential Measurements*, IEEE Transactions On Biomedical Engineering, Vol. 50, No. 3, March 2003.

[33] Pallás-Areny R., Webster J. G., *Common mode rejection ratio in differential amplifiers*, IEEE Transaction of Instrumentation and Measurement, vol. 40, pp.669 -676, 1991

[34] Johnson J. B., *Thermal Agitation Of Electricity In Conductors*, Physical Review, Volume 32, July 1928.

[35] Palmer R., *DC Parameters: Input Offset Voltage*, Application Report, Texas Instruments, 2001, Available http://www.ti.com/lit/an/sloa059/sloa059.pdf.

[36] Surtihadi H., Oljaca M., *Operational amplifier gain stability, Part 2: DC gain-error analysis*, Texas Instruments, Analog Application Journal, 2010.

[37] Ewing J. A., *Development of a Direct-Measurement Thin-Film Heat Flux Array, Master's Thesis*, Master's Thesis, Virginia Polytechnic Institute and State University, 2006.

[38] Völklein F., Blumers M., Schmitt L., *Thermoelectric microsensors and microactuators (MEMS) fabricated by thin film technology and micromachining*, 18th International Conference on Thermoelectrics, 1999.

[39] Knauss H., Gaisbauer U., Wagner S., Buntin D., Maslov A., Smorodsky B., *Calibration Experiments Of A New Active Fast Response Heat Flux Sensor To Measure Total Temperature Fluctuations - Part I. Introduction To The Problem*, Intern. Conf. on the Methods of Aerophys. Research: Proc. Pt. III. Novosibirsk, 2002, pp. 632–643.

[40] Agilent Tehcnologies, *Impedance Measurement Handbook*, 2nd edition, 2000.

[41] Belden, Detaileld specifications & Technical Data 9201 Coax-RG-58/U Type. http://www.belden.com/techdatas/metric/9201.pdf,

[42] Vaseghi V. S., Advanced Digital Signal Processing and Noise Reduction Second Edition, Chapter 2, Noise and distortion, John Wiley & Sons Ltd., 2000.

[43] Texas Instruments, Datasheet, *LMP2021/LMP2022 Zero Drift, Low Noise, EMI Hardened Amplifiers*, 2009, available http://www.ti.com/lit/ds/symlink/lmp2021.pdf, referred 19.12.2012.

[44] Texas Instruments, Datasheet, *OPA211-HT - 1.1 nV/√Hz Noise, Low Power, Precision Operational Amplifier*, 2012, available http://www.ti.com/lit/ds/symlink/opa211-ht.pdf, referred 19.12.2012.

[45] Analog Devices, Datasheet, *AD8628/AD8629/AD8630*, 2011, available http://www.analog.com/static/imported-files/data_sheets/AD8628_8629_8630.pdf, referred 19.12.2012.

[46] Analog Devices, Datasheet, *ADA4895-2*, 2011, available http://www.analog.com/static/imported-files/data_sheets/AD8628_8629_8630.pdf, referred 19.12.2012.

[47] Analog Devices, Datasheet, *ADA4528-1/ADA4528-2*, 2012, available http://www.analog.com/static/imported-files/data_sheets/ADA4528-1_4528-2.pdf, referred 19.12.2012.

[48] Linear Technology, Datasheet, *LTC1050 - Precision Zero-Drift Operational Amplifier with Internal Capacitors*, available http://cds.linear.com/docs/en/datasheet/1050fb.pdf, referred 19.12.2012.

[49] Linear Technology, Datasheet, *LTC1050 - Precision Zero-Drift Operational Amplifier with Internal Capacitors*, available http://cds.linear.com/docs/en/datasheet/1050fb.pdf, referred 19.12.2012.

[50] Maxim Integrated, Datasheet, *MAX44250/MAX44251/MAX44252*, August 2012, available http://datasheets.maximintegrated.com/en/ds/MAX44250-MAX44252.pdf, referred 19.12.2012.

[51] Texas Instruments, Datasheet, *TLC2652*, February 2005, available http://www.ti.com/lit/ds/symlink/opa211-ht.pdf, referred 19.12.2012.

[52] Intersil, Datasheet, *5V Ultra Low Noise, Zero Drift Rail-to-Rail Precision Op Amp - ISL28134*, 16.8.2012, avaible

http://www.intersil.com/content/dam/Intersil/documents/fn69/fn6957.pdf, referred 19.12.2012.

[53] Intersil, *HA-5147- 120MHz, Ultra-Low Noise Precision Operational Amplifiers*, 16.8.2012, avaible http://www.intersil.com/content/dam/Intersil/documents/fn69/fn6957.pdf, referred 19.12.2012.

[54] Analog Devices, Datasheet, *AD8421*, 2012, available http://www.analog.com/static/imported-files/data_sheets/AD8421.pdf, referred 19.12.2012.

[55] Analog Devices, Datasheet, *AD8229*, 2012, available http://www.analog.com/static/imported-files/data_sheets/AD8229.pdf, referred 19.12.2012.

[56] Texas Instruments, Datasheet, *INA128/INA129*, 2005, available http://www.ti.com/lit/ds/sbos051b/sbos051b.pdf, referred 19.12.2012.

[57] Linear Technology, Datasheet, *LTC1100 - Precision, Zero-Drift Instrumentation Amplifier*, available http://cds.linear.com/docs/en/datasheet/1100fc.pdf, referred 19.12.2012.

[58] Intersil, Datasheet, *40V Precision Instrumentation Amplifier with Differential ADC Driver*, 25.5.2012, available http://www.intersil.com/content/dam/Intersil/documents/fn69/fn6957.pdf, referred 19.12.2012.

[59] Maxim Integrated, Datasheet, *MAX4208/MAX4209*, April 2009, available http://datasheets.maximintegrated.com/en/ds/MAX4208-MAX4209.pdf, referred 19.12.2012.

APPENDIX I

Table I Test machine's main parameters [8].

Quantity	Value
Number of stator slots	12
Number of rotor poles	10
Winding factor of the fifth harmonic of the stator (the machine operates with the fifth harmonic)	0.933
Output power	37 kW
Speed	2400 min-1
Line-to-line terminal voltage in star connection	400 V
Winding turns in series per stator winding	64
Rated torque	147 Nm
Rated current	59–61 A
Length of air gap (on both sides of the rotor)	2.0 mm
External diameter of the stator stack	274 mm
Internal diameter of the stator stack	154 mm
Stator yoke height	21 mm
Thickness of PM	16 mm
PM remanent flux density, 20 ºC	1.1 T
PM remanent flux density, 80 ºC	1.03 T
Mass of magnets (NdFeB)	3.9 kg
PM resistivity	150 μΩcm

APPENDIX II

Calculations of sensor circuit's transfer function in figure x.x. Circuit is reformed and simplify with summing cable and amplifier capacitances as C_2 and then calculated parallel impedance C_2 with input resistance of amplifier R_3.

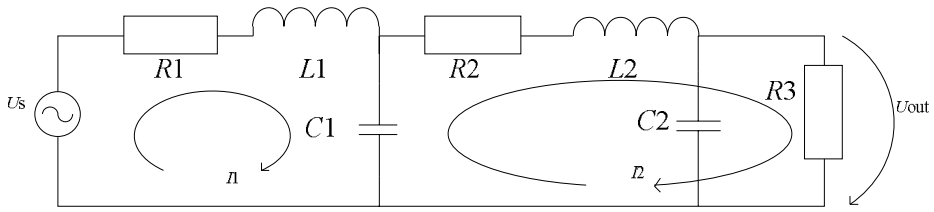

Closed loop current method is applied to circuit. By forming two current loops ***I*** and using Kirchhoff's voltage law, following matrixes are formed.

$$\boldsymbol{U} = \begin{bmatrix} U_s \\ 0 \end{bmatrix} \tag{II.1}$$

$$\boldsymbol{I} = \begin{bmatrix} I_1 \\ I_2 \end{bmatrix} \tag{II.2}$$

$$\boldsymbol{Z} = \begin{bmatrix} R_1 + sL_1 + \frac{1}{sC_1} & \frac{1}{sC_1} \\ \frac{1}{sC_1} & R_2 + sL_2 + \frac{1}{sC_1} + \frac{R_3}{sR_3C_2+1} \end{bmatrix} \tag{II.3}$$

By solving the current I_2, U_{out} can be calculated with combined impedance of C_2 and R_3.

$$\boldsymbol{U} = \boldsymbol{ZI} \tag{II.4}$$

$$\boldsymbol{I} = \boldsymbol{Z}^{-1}\boldsymbol{U} \tag{II.5}$$

$$U_{\text{out}} = I_2 \frac{R_3}{sR_3C_2+1} \tag{II.6}$$

And transfer function is received:

$$\frac{U_{\text{out}}}{U_s} = \frac{R_3}{\begin{matrix} s^4 + s^3\left(\frac{1}{C_2R_3} + \frac{R_1}{L_1} + \frac{R_2}{L_2}\right) + s^2\left(\frac{R_2}{C_2L_2R_3} + \frac{R_1}{C_2L_1R_3} + \frac{1}{C_2L_2} + \frac{1}{C_1L_2} + \frac{1}{C_1L_1} + \frac{R_1R_2}{L_1L_2}\right)\cdots \\ + s\left(\frac{1}{C_1C_2L_1R_3} + \frac{1}{C_1C_2L_2R_3} + \frac{R_1R_2}{C_2L_1L_2R_3} + \frac{R_1}{C_1L_1L_2} + \frac{R_1}{C_2L_1L_2} + \frac{R_2}{C_1L_1L_2}\right)\cdots \\ + \frac{R_1+R_2+R_3}{C_1C_2L_1L_2R_3} \end{matrix}} \tag{II.7}$$

APPENDIX III

fftalgo.m MATLAB code for FFT analysis for measured data.

```
% Fast fourier transform - Algorithm copied and modified from
%http://www.mathworks.se/help/matlab/ref/fft.html%
% calculating sampling frequency from the data imported data TEK00001
arvo1=TEK00001(1,1);
arvo2=TEK00001(2,1);
Fs=1/(arvo2-arvo1);     %sampling frequency

T = 1/Fs;                   % Sample time
L = length(TEK00001(:,2));    % Length of signal
t = (0:L-1)*T;                % Time vector
y = TEK00001(:,2);
NFFT = 2^nextpow2(L); % Next power of 2 from length of y
Y = fft(y,NFFT)/L;
f = Fs/2*linspace(0,1,NFFT/2+1);

% Plot single-sided amplitude spectrum.
figure
plot(f,2*abs(Y(1:NFFT/2+1)))
title('Single-Sided Amplitude Spectrum of y(t)')
xlabel('Frequency (Hz)')
ylabel('|Y(f)|')
```

APPENDIX IV

This appendix contains circuit and layout for the amplifier PCB with two channels. The circuit is in figure IV.1 and PCB layout in figure IV.2. The PCB was designed with Mentor Graphics PADS 9.3 software.

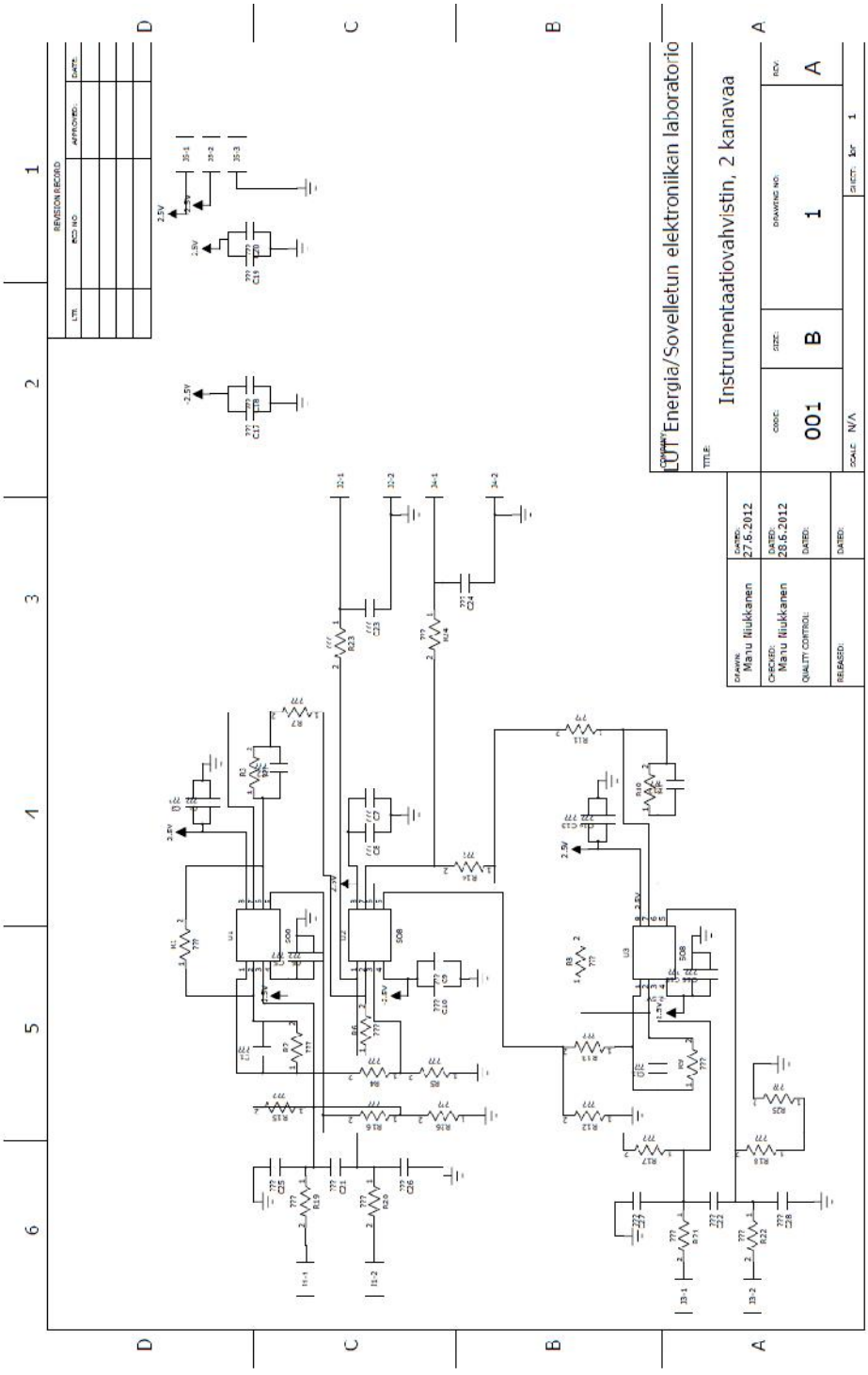

Figure IV.1 The circuit for a 2 channel instrumentation amplifier.

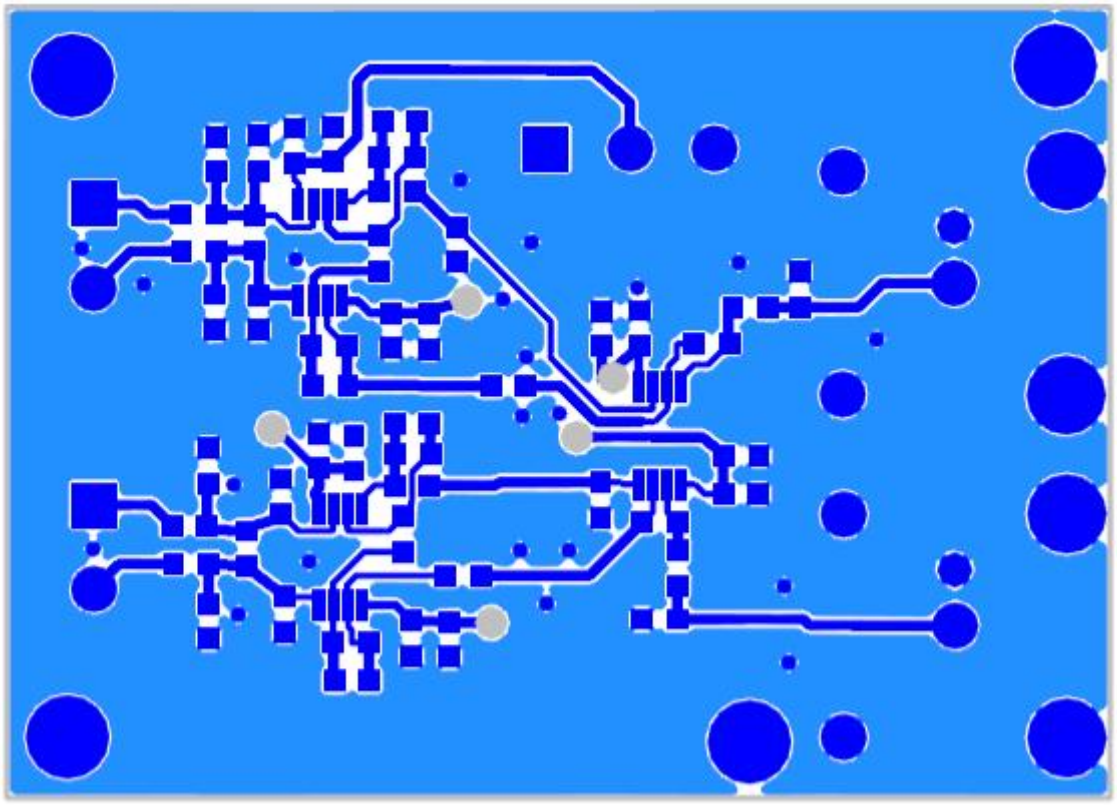

a)

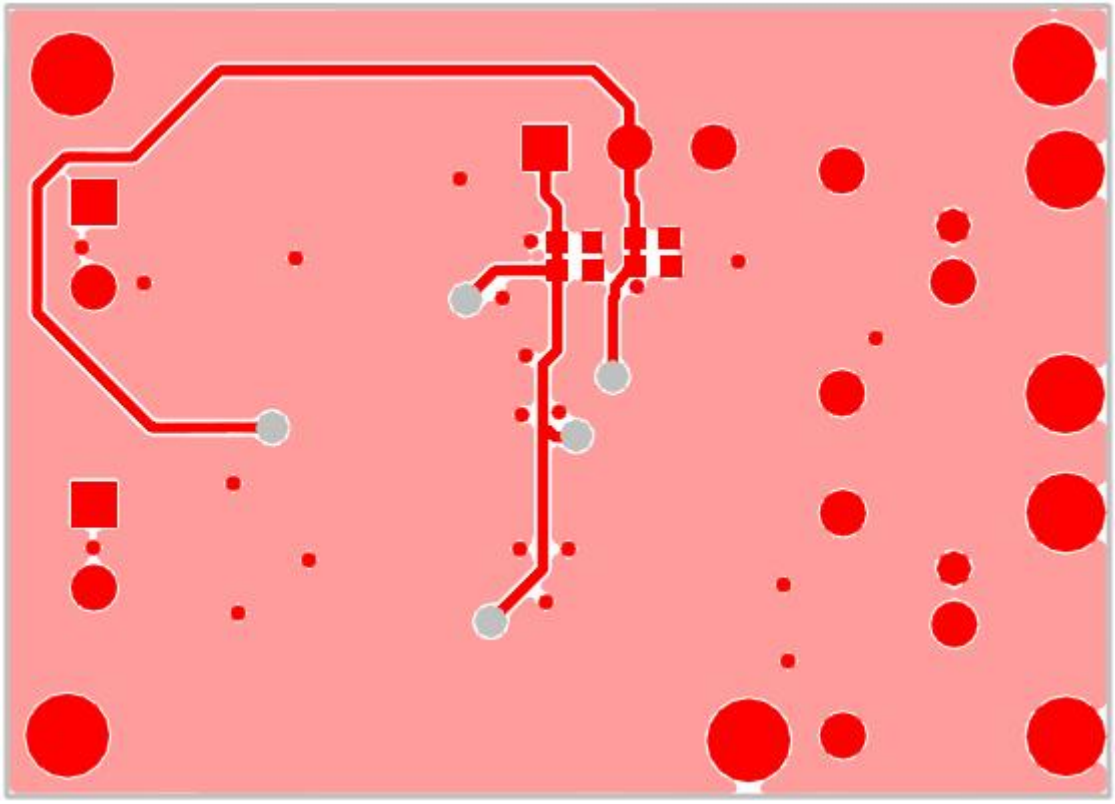

b)

Figure IV.2 The layout of the PCB where a) is top side and b) bottom side. The layouts are not in scale.